GPS estimates of ocean tide loading in NW-France: determination of ocean tide loading constituents and comparison with a recent ocean tide model

Mathilde Vergnolle, M. Bouin, F. Masson, Stéphane Durand, Jean-Marie Nicolas, S. Melachroinos, Laurent Morel

GPS estimates of ocean tide loading in NW-France: Determination of ocean tide loading constituents and comparison with a recent ocean tide model

Vergnolle, M.[1,*], M.-N. Bouin[2], L. Morel[1], F. Masson[3,§], S. Durand[1], J. Nicolas[1], S.A. Melachroinos[4]

1- Laboratoire de Géodésie et Géomatique (L2G), ESGT/CNAM, 1 Bd Pythagore, F-72000 Le Mans, France.

2- ENSG/LAREG/IGN, 6 et 8, Av. Blaise Pascal, F- 77455 Marne-la-Vallée, France.

3- Géosciences Montpellier, CNRS/Université Montpellier II, 4 place Bataillon, 34000 Montpellier, France.

4- GRGS/DTP/CNES, 18 Av. Edouard Belin, F- 31400 Toulouse, France.

**- Now at Laboratoire de Géophysique Interne et Tectonophysique, CNRS, OSUG, Univ. J. Fourier, Maison des Géosciences, BP 53, F-38041 Grenoble Cedex 9, France.*

§- Now at IPGS/EOST, CNRS/Université Strasbourg I, 5 rue Descartes, 67000 Strasbourg, France.

Accepted date. Received date; in original form date

Short title: GPS estimates of ocean tide loading in NW-France

Corresponding author: Mathilde VERGNOLLE

Phone: 00 33 4 76828089

Fax: 00 33 4 76 82 81 01

e-mail: mathilde.vergnolle@obs.ujf-grenoble.fr

SUMMARY

Ocean loading effects cause 3D displacements large enough to affect space geodesy measurements either at the sub-diurnal periods or at longer time scales by the means of spurious signals. GPS measurements, in turn, could provide local improvements of the models in coastal areas if their ability to precisely monitor such rapid displacements is assessed. In this paper, we use 105 days of continuous GPS measurements collected in 2004 in the French Brittany and Cotentin region to investigate: 1- the precision achieved by the GPS analysis on measuring 3D sub-diurnal displacements and amplitude and phase of the tidal constituents, 2- the quality of the most recent ocean tide model FES2004 in such a complex coastal context. Indeed, in this area, tide amplitudes are among the largest in the world (up to 16 cm of loading displacements on the vertical component) and are believed to show strong shallow-water tides. From a state of the art GPS analysis using the scientific GAMIT software over 2h sessions, we test two independent strategies for the realization of the reference frame. The position time series are then compared with the displacements predicted by the FES2004 model applied on an elastic Earth model. The two sets of results are consistent with each other at the same level of agreement than with the predicted displacements, namely 3 to 5 mm on the horizontal components, 10 mm on the vertical. This assesses the capability of this technique for measuring 3D ocean tide loading deformation. We validate the FES2004 model in the Brittany area, even though it slightly (2-7 mm) underestimates the 3 components amplitudes. With a harmonic analysis of the observed position time series, we obtain nevertheless an agreement at a sub-millimeter level for the M2, N2, O1, Q1 tidal constituents and at a millimetre level for the K1 and S2 tidal constituents. Moreover, we can extract a significant M4 load signal at the 95% confidence level from the GPS time series at the stations located in the Mont St Michel area. The detection of other shallow-water constituents would be helpful to understand the amplitude deficit between the FES2004 predicted and GPS observed displacements.

Key words: GPS – Ocean Tide Loading – Crustal Deformation - Brittany

1 INTRODUCTION

Atmospheric, hydrological, and oceanic mass transfers cause some important loadings of the Earth (e.g., Blewitt *et al.* 2001) and show some significant diurnal and seasonal position variations at the several millimeter level on the vertical component with mainly semi-annual and annual periods (Dong *et al.* 2002; Penna & Stewart 2003). On one hand, the knowledge of these loading effects, that affect GPS position estimates, has greatly improved since a few years (Blewitt *et al.* 2001; van Dam *et al.* 2001). Some atmospheric and hydrological loading estimations and ocean tide loading (OTL) prediction models are available to correct GPS position estimates either at the data processing stage, or at the time series interpretation stage. On the other hand, Penna & Stewart (2003) and Penna *et al.* (2007) showed that each unmodelled (sub-) daily periodic displacement can propagate into spurious long wavelength features in the GPS vertical position time series. The amplitude of the spurious signal strongly depends on the amplitude of the unmodelled displacements and on the site location. Penna *et al.* (2007) suggest vertical displacement errors up to about 12.5 mm, including up to 8 mm due to OTL mismodelling. Moreover, King *et al.* (2003) show that if both vertical OTL is not accounted for (or in a lower level, mismodelled) and the carrier phase ambiguities are not solved in GPS processing, the horizontal GPS positions may be biased by up to 40-50% of the vertical signal amplitude. Hence, unless using accurate ocean tide loading models in GPS processing, some spurious signal can bias the estimation of positions and velocities requested for high accuracy studies such as plate tectonics or reference frame realization. It is then important to evaluate the accuracy of the OTL models.

The OTL displacements are computed using an OT model and an Earth model. The accuracy of the OTL model is mostly limited by the accuracy of the OT model. Usually, OT model predictions are in good agreement in deep oceans but can differ in complex areas (i.e. complex coastal areas and complex continental shelves). In these areas, the production of OT model is more challenging than in deep oceans because sparse tide gauge data are used and global models could not integrate some local processes like wave interactions, strong bathymetric variations, and bottom friction phenomena (Dragert *et al.* 2000; Llubes *et al.* 2001). One possible way to improve OT or OTL models in these areas would be to integrate a new independent data set, such as GPS observations, in addition to data from tide gauges and altimetry (Dragert *et al.* 2000; Khan & Tscherning 2001; King & Aoki 2003).

The GPS technique has the potential to measure the OTL displacements as shown by several studies for the vertical OTL displacements (Baker *et al.* 1995; Khan & Tscherning 2001; Allinson *et al.* 2004; King *et al.* 2005) and by much fewer studies for the horizontal OTL displacements (Khan & Scherneck 2003). The question arising is to know if one can achieve a sufficient precision and accuracy on the 3D GPS OTL displacements to integrate them in OT model implementations or to constrain OTL models in the regions where models fail.

In this paper, to estimate the potential and the necessity of the GPS measurements to be integrated as constraints in future OTL models, we (1) evaluate the resolution and accuracy of the 3D OTL displacements derived from GPS observations, and (2) investigate the quality of the OTL displacements derived from the most recent OT model FES2004 (Lyard *et al.* 2006). To perform our goal, we use GPS data acquired in the Brittany-Cotentin region, in northwestern France, where the ocean tide amplitude is among the largest in the world. It is also a place where the ocean tide signal is influenced by a high coastal indentation in Brittany, and by strong local shallow-water tides. The large amplitude and complexity of the OT makes this region an area of great interest to measure OTL displacements and validate predicted ones.

In the following, we first describe the NW-France ocean tide loading campaign (section 2), and the FES2004 OT model (Lyard *et al.* 2006) and derived OTL model (section 3). We then define a valid network processing strategy (section 4) that allows one (1) to accurately measure the 3D OTL displacements in a global reference frame, (2) to extract the major tidal OTL constituents (semi-diurnal and diurnal ones) as well as higher frequency terms, and (3) to directly compare observed and predicted OTL displacements (section 5).

2 NW-FRANCE OCEAN TIDE LOADING CAMPAIGN

In Europe, ocean tides are the strongest on the Atlantic and Channel coasts. Their amplitude can reach 14 m in Cotentin and Brittany, which induces 5 to 16 cm vertical crustal peak-to-peak displacements and about one third of this displacement on the horizontal components. Figure 1 shows the vertical displacements due to the M2 load, main tidal constituent in the studied area, from FES2004 (Lyard *et al.* 2006). Moreover, due to the weak bathymetric variations and to the short wavelength geometric features of the coastline, the shallow-water tides are amplified in this coastal area. Hence, OTL

displacements are high enough to be measured in this region, as well as could be the energic shallow-water constituents of the ocean tide loading although they are usually difficult to characterize.

In 1998 and 1999, GPS and gravimetry data sets were used to study the OTL effects in Brittany (3-4 days, Vey *et al.* 2002; Llubes *et al.* 2001). The gravimetric analysis (Llubes *et al.* 2001) showed a good correlation but an amplitude discrepancy of 16% between the observed and predicted signals at Brest (BRST, Fig. 1). The GPS analysis (Vey *et al.* 2002) showed that the amplitude of the signal is large enough to be measured by GPS but that the data set was too short to validate models. To go further in the study of the OTL effects in Brittany-Cotentin, a new multi-geodetic-technique campaign (GPS, absolute and relative gravimetry, inclinometry, tide gauges, satellite laser ranging) took place from March to October 2004 (Llubes *et al.* revised).

In this paper, we focus on the results of the GPS campaign. Twelve GPS stations collected data from March to June 2004 during 105 days in addition to 3 stations of the French GPS Permanent Network (RGP) located in the studied area (Fig. 1). Most of the campaign stations were installed on the north coast where ocean tides are the most significant. The other stations were installed on the south coast and inland to observe the Earth crust's response to the propagation of the main load.

3 OCEAN TIDE AND OCEAN TIDE LOADING MODELS

Owing to the availability of TOPEX-Poseidon altimetry data in the 1990s and to the effort undertaken by the tidal scientific community to develop new tidal models, the accuracy of OT models has greatly improved (Andersen *et al.* 1995; Shum *et al.* 1997; Baker & Bos 2003; Andersen *et al.* 2006). It now reaches a centimeter level accuracy in the deep ocean. A new release of the FES tidal atlas was recently produced, namely FES2004 (Lyard *et al.* 2006). It is computed from tidal hydrodynamic equations and from data assimilation based on the same modelling approach as FES99 (Lefèvre *et al.* 2002). With a better discretization of the finite element grid, in particular near the coastal areas, and the introduction of loading and self-attraction terms in the tidal equations, the French Tidal Group was able to better compute the hydrodynamic solutions for shelf areas, especially on the Atlantic ocean. Moreover, the assimilated data set, including tide gauge data, TOPEX-Poseidon and ERS altimetric data, increased since the previous FES2002 release (Lyard *et al.* 2006). Comparisons of the FES2002 model, the GOT00.2 model (Ray 1999), and the new FES2004 model with tide gauge data show an

improvement of the FES2004 model of about 10 to 30% for the semi-diurnal constituents (except K2) with respect to the 2 other models (Lyard *et al.* 2006). Comparison of FES99 (Lefèvre *et al.* 2002) and FES2004 models with altimetric data (Jason-1 and ENVISAT data) also shows an overall improvement of FES2004 model (12% and 7% respectively). The major improvement in FES2004 comes from a better accuracy of the prediction of the tidal constituents in coastal and continental shelf areas (about 30% compare to Jason-1 data) without decreasing accuracy in the deep ocean.

To predict the OTL displacements, an OT model and an Earth model are required. The OTL effects are described by the convolution between the surface mass load derived from the OT model and Green's functions, which are a linear combination of load Love numbers, describing the response of the Earth model to that load (e.g., Farrell 1972). The accuracy of the OTL displacements greatly depends on the accuracy of the OT models. We chose to compare the 3D observed OTL displacements derived from the GPS data to the 3D predicted OTL displacements derived from FES2004 OT model (Lyard *et al.* 2006) because FES2004 is the most recent ocean tide model available. Moreover, it clearly tries to better reproduce ocean tides in hydrodynamically complex coastal regions like Brittany–Cotentin.

We want to investigate the accuracy of the OTL model in quantifying the quality of the main predicted constituents as in classical OTL analysis but also in estimating the quality of the 3D OTL predicted displacements to provide quantitative information on the accuracy of the OTL correction used in standard GPS analysis. For that latter purpose, we build the 3D OTL predicted position time series. Eleven tidal constituents are classically used by GPS software routines correcting OTL effects, namely M2, S2, N2, K2 for the semi-diurnal ones, K1, O1, P1, Q1 for the diurnal ones, and Mf, Mm, Ssa for the long period ones. We use these terms to compute the 3D OTL predicted position time series in order to be consistent with standard GPS analysis and represent as closely as possible the complete observed signal. In FES2004, they are provided on a regular rectangular grid of 1/8 degree which corresponds to cells of 13.8 km by 9.3 km at the latitude of our study which is much better than the resolution provided by other OT models (McCarthy & Petit 2004). We get the site-dependent amplitude and phase values corrected for the center of mass motion of the Earth due to ocean tides for the 11 tidal constituents from the Bos and Scherneck OTL Provider (http://www.oso.chalmers.se/~loading/). The coastline used is the one of the Generic Mapping Tools package (P. Wessel and W. H. F. Smith, http://gmt.soest.hawaii.edu/) with a spatial resolution better

than 500 m. We then compute the OTL vertical and horizontal displacements with the Fortran routine hardisp.f of D. Agnew based on his former routine distributed with the SPOTL software ("Some Programs for Ocean-Tide Loading", Agnew 1996, 1997) which use the elastic Green's functions based on the Gutenberg-Bullen Earth model. This procedure is the one chosen by IERS for their standards (McCarthy & Petit 2004).

4 DATA PROCESSING

To measure the OTL displacements, we implement a GPS processing strategy that provides precise sub-daily positioning without smoothing the researched signal. In order to compare our observed OTL position time series to predicted OTL position time series, we define an OTL reference frame (hereafter referred as OTL RF). The Datum's stability is assessed by implementing two end-member strategies to express the final GPS position time series. In this section, we first present the common processing parameters used in both end-member strategies; second, the OTL reference frame; then the two end-member strategies; and finally the evaluation of the quality of the solutions.

4.1 COMMON PART OF THE PROCESSING STRATEGIES

We analyze the continuous GPS data of eleven of the twelve campaign sites and of three RGP permanent stations (Fig. 1) from March to June, 2004, using the GAMIT 10.21 software (King & Bock 2005). Indeed, since the FLER station, in Cotentin (Fig. 1), showed some monument stability problems, we removed its data in the final GPS analysis presented here. In order to decorrelate the tropospheric parameter estimation from the vertical positioning within the GPS processing, our stations are included in a regional network with baselines longer than 500 km (Tregoning *et al.* 1998; Duan *et al.* 1996). The reference frame stabilization of our network is achieved through the use of 16 European stations from the IGb00 reference network (BOR1, BRUS, GLSV, GRAS, GRAZ, HOFN, MAS1, MATE, NICO, ONSA, TRAB, TRO1, VILL, WSRT, WTZR, ZIMM) (Altamimi *et al.* 2002; Ferland 2003). Most of the processing parameters are classically chosen: Solid Earth tides, pole tides, and high frequency tide corrections were applied following the IERS 2003 standards (McCarthy & Petit 2004), as well as IGS antenna phase center models. As the periods of the two main ocean tide constituents (M2 and S2) are close to 12h, short session lengths are necessary to prevent over-

smoothing of the signal under investigation. We test different session lengths between 1 and 4h and find that 2h sessions are a good trade-off between motion sampling and position precision. To sample the short term displacements as well as possible, we process overlapping 2h sessions every hour, resulting in 24 position estimates per day for every station. Tropospheric delays are estimated every 30 min in 2h sessions. The a priori values coming from the Saastamoinen model (Saastamoinen 1972) and the Niell (1996) hydrostatic and wet mapping functions are used. The IGS final orbits and the IERS USNO Bulletin B Earth Orientation Parameters (EOP) are kept fixed in the processing. A priori station positions were derived from ITRF2000 for the reference stations and from a first run of adjustment with a free network processing using 24h sessions for the Brittany sites. Both a priori position sets are corrected from OTL effects using the FES2004 model, as described in the previous section, in order to start our analysis with values as accurate as possible. The constraints we apply on the a priori positions of the IGS and Brittany stations depend on the implemented strategy to tie the GPS solution to the OTL RF defined in the following section.

4.2 THE OTL REFERENCE FRAME

Previous OTL studies using double difference based GPS softwares present relative GPS solutions (in a local reference frame). The station position variations are expressed relatively to one or more inland stations with fixed coordinates in a global reference frame (e.g., Khan & Tscherning 2001; Vey *et al.* 2002). This strategy, even if straightforward, has one major drawback. Such relative position variations are not directly comparable to other geophysical results or to OTL models. The only rigorous way to make these comparisons is to express GPS results in a global reference frame, consistent with global OTL models. We therefore define a reference frame, consistent throughout our whole experiment, transforming our GPS position estimates into ITRF2000 positions corrected from the OTL effects deduced from FES2004. Our reference frame, the OTL RF, is therefore defined as ITRF2000 positions and velocities corrected from the FES2004 OTL effects. The consistency level of this reference realization will be directly related to the accuracy of the FES2004 OTL predictions for the IGS stations (as IGS stations only are used in the RF definition). From the common strategy, we test end-member processing strategies to tie the GPS solution to the OTL RF from a constrained solution (St1 strategy) and a free network solution (St2 strategy). The comparison of the final solutions will allow us to evaluate the stability of the GPS solutions and the quality of the OTL RF realization.

4.3 THE “CONSTRAINED” SOLUTION (St1 STRATEGY)

The St1 strategy ensures the reference frame stability by applying very tight constraints (1 mm on every component) on the IGS sites used. The reference frame consistency throughout the whole experiment period (3.5 months) is therefore assessed in the GPS processing itself. Such a constraint level requires the correction of a priori positions with a level of confidence better than 1 mm. We then assume that the FES2004 model provides a prediction of OTL effects accurate at a millimeter level on the IGS sites. In this St1 strategy, the constraints applied on the a priori positions of the Brittany-Cotentin sites are 5 cm on the horizontal components and 10 cm on the vertical component.

4.4 THE “FREE NETWORK SOLUTION” (St2 STRATEGY)

The St2 strategy involves a free network analysis with looser constraints on every site with respect to the St1 strategy. The free network solution (before the reference frame realization step) should not be influenced by the a priori positions. The constraints applied on these a priori positions must be loose enough to not bias the intermediate free network results. From a theoretical point of view, this could be easily achieved by choosing constraints (i.e. a priori standard deviations) one order of magnitude larger than the GPS phase a priori standard deviation. Therefore, we ensure that the solution is more weighted by the normal equations than by the constraint equations on the positions. In the GAMIT software, the default value for the phase a priori standard deviation is 10 mm (basically 2 mm for each observation, changed to 10 mm to account for the correlation between successive observations) (King and Bock, 2005). Constraints of 5 to 10 cm on the a priori positions should then be loose enough to avoid any strong influence of these positions on the free network solution. To check this assumption, we test several levels of constraints applied to the a priori positions of IGS and Brittany stations. With constraints of 1 cm/5 cm on the horizontal and vertical a priori positions respectively on the IGS sites (5 cm/10 cm on the Brittany sites), a clear correlation is observed between free network positions and the a priori constraints. This correlation is observed on every IGS station and increases for the remote sites located at the edge of our network. With looser constraints on a priori positions (5/10 cm for the IGS station and 10/20 cm for the Brittany stations), this behaviour is not reproduced anymore. We conclude that, in agreement with the theory, constraints of 5 to 20 cm are loose enough to estimate free

network positions without any strong influence of the a priori constraints. We use this level of constraints in the following work.

We then realize the reference frame by minimizing the position deviations of the IGS stations included in the GPS processing with respect to the OTL RF. To do this, we estimate the parameters of a Helmert transformation between our individual coordinate sets and the OTL RF on the IGS stations, using the GLOBK software (Herring *et al.* 1990; Herring 2003). Taking into account the regional distribution of the network, we calculate a three parameters transformation (three translations) and not a transformation with more parameters (scale, rotation). In order to estimate the robustness of our reference frame realization, we made some tests on the final results to evaluate the influence of the reference station selection. We conducted these tests on a 20 day time series (480 individual solutions). Different sets of IGS reference stations were used. The stations we removed were chosen according to their residuals in the least squares reference frame definition process. The first set of stations (R1 hereafter) includes all the 16 IGS stations we processed along with our network stations. We then remove one after the other the 6 following remote stations sorted by increasing quality: TRAB (set R2), MAS1 (R3), NICO (R4), TRO1 and HOFN (R5), and GLSV (R6). The last set R6 includes 10 stations only (the original 16 ones minus the 6 above stations). The root mean square (RMS) of the reference frame stabilization (calculated over all the stations used and their components) is not very good when we keep the 16 IGS station as reference frame stations (R1). In particular the north and east RMS at the remote stations are generally higher than 10 mm. With respect to the R1 set, the RMS of the reference frame stabilization improves of 9.5% (R2), 18% (R3), 22.5% (R4), 46% (R5), and 52% (R6). In addition to this RMS decrease, the adjustments on the 10 European IGS stations kept as reference frame improve greatly in R6 with respect to R1. The mean North, East, and Up (NEU) RMS (average on every reference station per component) improve of 38%, 32%, and 42% with respect to the R1 set. These tests show that the realization of the OTL RF with 2h session data is better when we exclude the remote stations of the stabilization process.

4.5 QUALITY OF THE St1 AND St2 SOLUTIONS

As already emphasized, precise determination of station positions with short sessions requires correct zenith tropospheric delay (ZTD) estimation (Khan & Scherneck 2003) along with the correct fixing of phase ambiguities to integer values (King *et al.* 2003; Vey *et al.* 2002). With a network that includes

the 16 IGS stations in addition to the 14 Brittany stations, baseline lengths range from 40 km to 5070 km, 58% of them being shorter than 1500 km. The number of carrier phase biases fixed on 2h sessions in St1 and St2 strategies is respectively 60% and 64% which depends on the geometry of the network. We also checked the final correlation between ZTD estimations and the observed vertical displacements. For both strategies, the correlation is very small, less than +/- 0.06 for most of the stations (29 over 30 for St1 strategy, and 25 over 30 for St2 strategy). Few exceptions exist for the furthest stations where the correlation coefficient can reach up +/- 0.2. Nevertheless, this value is still low and reasonable, showing that there is no trade off between the ZTD and the vertical displacement estimations in our processing. No significant vertical motion being absorbed into the ZTD, we therefore validate the constraints applied to the vertical component.

To evaluate the quality of the reference frame realization, we first compare the St1 and St2 results with the FES2004 predicted OTL displacements on the IGS stations used as references. The agreement between St1 results and the OTL predictions is excellent (RMS lower than 0.6 mm on each component), reflecting the 1 mm constraints we imposed on these stations within the GPS processing. We expect a lower agreement between the St2 results and the OTL predictions on the IGS stations, as we do not constrain the position but calculate a translation parameter transformation to express the GPS solution in the OTL RF. We obtain mean RMS on the 10 IGS stations (R6) of 3.2, 3.1, and 9.7 mm on the NEU components, respectively. These values reflect a good consistency of the St2 session to session RF realization. We then compare the Brittany site position time series resulting from St1 and St2 strategies. They are in good agreement with weighted root mean squares (WRMS) of 3.4, 4.0, and 9.4 mm on the NEU components respectively, which are consistent with the formal error level (see section 5). These results show first that, in both strategies, the realization of the OTL RF is achieved successfully and second that, under the assumption that FES2004 is valid at the millimeter level for IGS stations, we can consider that we do not miss any oceanic signal in the position time series at the precision level of the observations.

5 GPS OBSERVED OTL DISPLACEMENTS AND COMPARISON WITH PREDICTED OTL DISPLACEMENTS

We obtain 105-day time series for the 30 stations included in the processing. In this section, we focus on the results obtained for the 14 stations located in the studied area (Fig. 1). We present first the 3D position estimates with an accuracy assessment, and then a spectral and a harmonic analysis. At both stages, we compare the estimations with the predictions.

5.1 POSITION TIME SERIES ANALYSIS

At Cherbourg (CHER, Fig. 1), two inclinometers, an absolute gravimeter and a relative one were installed close to the GPS station. In addition, the GPS results obtained at Cherbourg are representative for the whole network. We therefore present, as an example, the results at this station. Figure 2 shows the observed 3D position time series at CHER without any a posteriori filtering or a posteriori outlier cleaning. The formal errors on the NEU position estimates are 6, 3 and 10 mm for the St1 solution, and 3, 3 and 10 mm for the St2 solution. These values are mean values but show a great consistency over the 14 stations. When processing 2h sessions, we obtained solutions with 3D formal errors at the millimeter to centimeter level, close to the level of precision of classical 24h session solutions. These formal errors are always smaller than the amplitude of the signal even on the horizontal components which allow us to be confident in the horizontal results. The position time series we obtain from the two strategies clearly show surface displacements caused by the oceanic loading not only on the vertical component – as already extensively shown in previous studies (e.g. Dragert *et al.* 2000; Khan & Tscherning 2001; Allinson *et al.* 2004; King *et al.* 2005) – but also on the horizontal components (Khan & Scherneck 2003) at all the regional stations with peak-to-peak amplitudes that range from 8 to 40 mm depending on the station.

To investigate the consistency of the two observed solutions, we perform a residual analysis at all the stations on each component based on the mean differences and the weighted standard deviations of the differences (WSDD) between the two solutions. The mean differences range from -0.18 to 0.16 mm on the vertical component (respectively from -0.28 to 0.03 mm on the N component, from -0.04 to 0.05 mm on the E component) between the two solutions, demonstrating that no significant bias is observed between our two strategy results. The NEU WSDD (Table 1) show values consistent with the errors

previously estimated (e.g., WSDD of 3.3, 4.1, and 8.3 mm at CHER on NEU component respectively). This result ensures consistent independent GPS solutions at the millimeter level.

We perform the same analysis between the observed displacements and the predicted displacements and find roughly the same level of agreement between the different time series (Table 1). The St1 and St2 observed displacements are closer together than with the prediction, except on the east component (see St2/model WSDD with respect to St1/St2 WSDD in Table 1). The lower agreement of the observed solutions on the east component could reflect a better position estimation on the north component than on the east component. This is classically the case in standard GPS processing (Melbourne 1985; Blewitt 1989) but amplified in our study because of the short session length. Though non significant regarding the precision of the observations, we note a small systematic bias between the observed and predicted displacements. Whatever station considered, the predicted signal amplitudes are systematically smaller than the observed ones with a difference of 2 to 7 mm on each component (Fig. 2).

The comparisons between the observed OTL signals and between the observed and predicted OTL signals show an overall good agreement at the positioning level of precision of 3 to 6 mm on the horizontal component and about 1 cm on the vertical component. This result allows us to validate the FES2004 OT model, at least in west of France, for applications such as meteorological applications that require to know OTL effects with an accuracy better than 3 cm to estimate realistic GPS-derived precipitable water vapor (Vey *et al.* 2002). However, we suggest that the predicted displacements derived from the FES2004 OT model are slightly underestimated on the three components. In the next step, we perform a spectral and harmonic analysis thanks to which we deeply examine the discrepancy between observed and predicted OTL displacements.

5.2 SPECTRAL AND HARMONIC ANALYSIS

We first perform a spectral analysis on the St1 and St2 strategy time series to assess the noise level of our harmonic analysis. Figures 3 and 6 represent the amplitude spectrum. We find that the noise level is about the same at different stations as shown for the vertical component at CHER (Fig. 3), MALO, DUCE, and COUT (Fig. 6). The standard deviation (i.e. noise at the tide-free frequencies excluding frequencies from S2 to N2 frequencies) ranges from 0.2 to 0.6 mm on the NEU components for CHER for both observed solutions (Fig. 3).

We then perform a harmonic analysis on the St1 and St2 strategy time series as well as on the predicted time series using the T_TIDE package (Pawlowicz *et al.* 2002), already used in other ocean tide loading studies (e.g., King *et al.* 2005). The observed times series at RENN, TREV and SURZ show gaps of long duration (16, 34, and 48 days respectively). Although one third and one half of the data are missing at TREV and SURZ, we still decide to perform the harmonic analysis of these time series because there are the only stations on the south coast of Brittany. The results at these stations should therefore be regarded with caution. As already noticed by Khan & Tscherning (2001), we are not able to separate constituents that have very close periods like K2 (11.97h) and S2 (12.00h), or P1 (24.07h) and K1 (23.93h) with 105 day time series. These authors suggest that the separation of these waves requires at least 6 months of continuous data, i.e. twice the number of data we get. We then extract only 3 semi-diurnal (M2, S2, N2) and 3 diurnal (K1, O1, Q1) tidal constituents from both the observations and the prediction. The results are shown in Tables 2 and 3 in terms of amplitude and phase consistencies for each station. The amplitudes and phases on the NEU components, for the BRST and CHER GPS stations are shown on Figure 4. We choose BRST because it is localized where the loading amplitude of M2 is the highest, and CHER for its representativeness of the whole network. The confidence intervals are calculated using a bootstrap analysis, based on a coloured-noise model (Efron & Tibshirani 1993). Among the 6 tidal constituents, the loading amplitude of M2 at all the regional stations is the highest but all the 6 considered tidal constituents can be well extracted (Table 2, Fig. 4). On the 6 tidal components, the 95% confidence level ranges from 1 to 2 mm on the vertical component and is below 1 mm on the horizontal components which is fully consistent with the noise level extracted from the amplitude spectrum. Figure 5 shows, for each station, the 3D misfit between the different solutions, two by two, as the root mean square of the sum of the squares of the complex differences for the 3 components and the 6 constituents (King et al. 2005; Thomas et al. 2007). The 3D misfit, over the 6 constituents, should reflect the agreement between the two observed position time series and between the observed and predicted position time series (section 5.1). It is slightly lower than the discrepancy shown between the position time series. The analysis of the 6 main constituents may not be enough to assess the quality of the OTL predictions.

The consistency of the M2 amplitude is very good between the two observed solutions and the prediction (Tables 2 & 3, Fig. 5). For the M2 constituent alone, the 3D misfit shows an agreement better than 1 mm on the NEU components between the two observed solutions for all the stations

except TREV and SURZ that suffer of a limited number of data. Indeed, the amplitude differences are less than 0.5 mm on the N and E components, and less than 1 mm on the vertical component (Table 2), and the phase differences are negligible regarding the phase precision (1 to 5° on the NEU components at 95% confidence level, Table 3). Despite the 3D misfit being higher between each observed solution and the predictions, it is still better than 3 mm (Fig. 5). On the U component, we observe a systematic positive phase lag of 3 to 9° between observations and prediction (except BAYE). On the horizontal components, this phase lag ranges from -3 to -10°, close to the significancy limit. We conclude that the agreement of the model with our observations on the M2 constituent is very good in amplitude, whatever the component considered, with a small phase lag.

For the other diurnal and semi-diurnal constituents with smaller amplitudes, the agreement between the observations together and with the prediction is of the same level as for M2, except for the K1 constituent (Fig. 5). The amplitude differences between the predicted and observed solutions are below 0.5 mm on the N and E components, and below 1mm on the vertical (with the exception of the K1 and S2 terms, Table 2). Except for some specific constituents (K1 vertical component and Q1), the phase agreement between observation and prediction is good with discrepancies below 15°. The phase standard deviation for each tidal constituent and component are also usually small, similar to the ones found for M2 in Khan & Scherneck (2003), and smaller than the ones found by King et al. (2005).

Looking carefully at the results, we find a less good agreement between the observed and predicted K1 constituent and between the two S2 estimations in comparison with the agreements on the other constituents. Some incoherent signals found in GPS observations at near solar and sidereal frequencies could be attributed to orbit perturbations or multipath, as already emphasized in several studies (Rothacher *et al.* 2001 ; Scherneck *et al.* 2000). This could explain the strong disagreement between the observed and predicted K1 amplitude and phase, mostly on the vertical component (Table 3 and Fig. 4). The S2 constituent estimation (on the vertical component) can also be affected by satellite orbit errors propagating on the K2 constituent, the S2 and K2 constituents being difficult to separate. However, because it is a disagreement between the two S2 estimations (and not with predicted S2), we suspect that it is partly due to a mis-estimation of the zenithal tropospheric delay (ZTD). Indeed, at all the stations, we find a signal whose amplitude ranges from 1 to 2.2 mm in the St2 ZTD time series at the S2 constituent period. We do not find any equivalent signal in the St1 ZTD time series. Moreover,

the S2 constituent estimation from the St1 solution agrees better with the prediction than the S2 constituent estimation from the St2 solution.

In this study, the precision on the phase estimate is about the order of the phase difference found for each tidal constituent and component. The levels of agreement in phase as well as in amplitude are consistent with the 3 to 10 mm precision we obtained in the 3D time series. The quality of the model predictions cannot be investigated beyond this limit.

5.3 DETECTING SHALLOW-WATER LOADING CONSTITUENTS.

One of the reasons why we study ocean loading in Brittany-Cotentin is that the shallow-water tides are supposed to be very energetic in this area, in particular in the Bay of Mont St Michel and surroundings (location of MALO, DUCE, and COUT stations). For example, the amplitude of the M4 tide exceeds 30 cm (Lyard *et al.* 2006; Andersen *et al.* 2006) and the amplitudes of MS4 and M6 tides exceed 15 cm (Andersen 1999). According to the M4 tide that is included in the FES2004 model (Lyard *et al.* 2006), the predicted amplitude of the M4 load can reach 1 mm in the Mont St Michel area. We now specifically look if the GPS tool is capable to detect this short period tidal constituent in 105-day GPS time series.

We perform a spectral and harmonic analysis on the vertical position time series at MALO, DUCE, and COUT (Fig. 6 and Table 4). We can extract the M4 loading constituent from the St1 and St2 observations at MALO with a signal-to-noise ratio of 1.4 and 1.3 respectively. The estimated amplitudes are 1.30 +/- 1.12 mm and 0.85 +/- 0.76 mm (95% confidence) with estimated phases of 165.2 +/- 57.5° and 151.4 +/- 59.5° (95% confidence) from the St1 and St2 solutions respectively. The noise level on the vertical component at MALO is 0.53 mm and 0.46 mm from the St1 and St2 solutions respectively, consistent with the values we obtain for the 95% confidence level on the M4 loading constituent estimation. St1 and St2 M4 loading constituent estimations are consistent. They are also consistent with the predicted loading constituent derived from FES2004 (Table 4). Finally, their amplitude is almost as large as the Q1 loading amplitude (Tables 2 and 4). The M4 loading constituent estimation at DUCE and COUT, also located in the bay of Mont St Michel, is not as well determined as the estimation of M4 loading constituent at MALO. It is significant only at the 68% confidence level (Table 4). However, the estimated amplitude is in good agreement with the predicted one at these locations (Table 4). We then suggest that this short period signal, despite its small

amplitude, can be measured on continental shelves such as the Brittany-Cotentin shelf where high wave interactions occur.

We can also extract two other shallow-water loading constituents (S4 and SK3) on most of the vertical time series with signal-to-noise ratio higher than 1. Because these shallow-water loading constituents are combinations of S2 and K1 loading constituents and mostly because we found them at most of the sites, we suspect that these signals can be due to artefacts of the GPS processing. They might be attributed to multipaths that could affect the GPS signal at all the integer fraction of the K1 period (e.g., Ragheb *et al.* 2007) and to periodic orbital error at integer fraction of the orbital period (Khan & Scherneck 2003). Finally, shallow-water loading constituents like M3 or M6 are close to be detected but still suffer from a high noise at high frequency to be accurately extracted. Nevertheless, if the GPS tool were able to extract all the shallow-water loading constituents, their sum would exceed the amplitude of some diurnal constituents in this region (e.g., O1, Q1). In that case, the shallow-water cumulative amplitude could partly fill the amplitude deficit between the observed and predicted loading signal (section 5.1). These short period constituents would then be important to account for in hydro-dynamically complex region as the Brittany-Cotentin in order to improve the accuracy of the OTL signal. We hope to be able to confirm this hypothesis with the analysis of the gravimetry data at CHER since shallow-water loading signals have already been detected with superconducting gravimeters in Europe (Boy *et al.* 2004) and in Japan (Khan & Høyer 2004).

6 CONCLUSION

We show that GPS is able to measure the sub-daily OTL displacements not only on the vertical component but also on the horizontal components with 10 mm precision on the vertical positioning and 3 to 6 mm precision on the horizontal positioning. We can extract the M2 and N2 semi-diurnal and O1 and Q1 diurnal constituents with a precision better than 1 mm at a 95% level confidence on the NEU components, consistent with the noise level derived from the amplitude spectrum (0.2 to 0.6 mm on the NEU components). The estimation of the K1 and S2 constituents is more delicate because it potentially suffers of problems related to satellite orbit errors or troposphere. Finally, we are able to extract the M4 load signal at 95% confidence level from the 105 day observed time series in the area of Mont St Michel, at MALO, where the M4 predicted loading amplitude can reach 1 mm. This result

is encouraging for the detection of shallow-water loading constituents with amplitudes higher than 0.5 mm.

We validate the prediction derived from the new FES2004 OT model (Lyard *et al.* 2006) in this Brittany-Cotentin complex region. We conclude from our analysis that the OTL model is valid at the precision level of the GPS measurements in this area. However, we suggest, from the systematic difference between the observed and predicted displacements, that the latter are slightly under-estimated on the three components. We exclude a strong mismodelling of the M2 constituent (main tidal constituent in the area), the NEU amplitude predictions of M2 being consistent with the observations (3D misfit of 2-3 mm, Fig. 5). We propose that the discrepancy could be due to a weak GPS estimation of some ocean tide constituents, like K1, and a lack of modelling (or mismodelling) of the shallow-water tides in OTL models. However, based on the estimation of the M2, S2, N2, and K1 constituents derived from the GPS data of the 8 stations located on the north coast of Brittany, Melachroinos *et al.* (2007) show that, among six global and one regional OTL models, FES2004 OTL predictions, along with the regional model predictions, best fit the observations in this complex region. Finally, owing to the expression of the time series in a global reference frame and to the fruitful attempt to extract some shallow-water loading constituents, this analysis raises again the question of the integration of some GPS measurements as additional data in OT models where altimetric or tide gauge data are lacking or as additional data in OTL models used to correct GPS processing dedicated to atmospheric, meteorological, or Earth deformation studies.

ACKNOWLEDGEMENTS

We thank N. Florsch (University Paris VI) and M. Llubes (LEGOS), the PIs of the ocean tide loading Brittany campaign performed in 2004, as well as the GDR G2 (Geodesy-Geophysics) which financed the campaign. We are grateful to P. Collard, J. Kieffer (Géosciences Montpellier), and J. Cali (L2G) for their contribution to the installation of the GPS sites. We acknowledge the INSU and the LDL for the use of their GPS receivers. We are grateful to all the people who accepted to welcome the GPS receivers during the campaign. The authors wish to acknowledge helpful discussions with O. Francis and T. Van Dam (Univ. of Luxembourg), and O. de Viron (IPG Paris). Insightful reviews by P. Clarke and an anonymous reviewer significantly helped improve the manuscript. A great part of this work

was supported by the Region Pays de la Loire which financed a post-doctorate as well as computing equipments. We acknowledge the Bos and Scherneck OTL provider for providing the amplitude and phase coefficients of the tidal constituent used in this study.

REFERENCES

Agnew, D.C., 1996. SPOTL: Some programs for ocean-tide loading, *SIO Ref. Ser.*, 96-8, 35pp., Scripps Inst. of Oceanogr., La Jolla, California.

Agnew, D.C., 1997. NLOADF: A program for computing ocean-tide loading, *J. geophys. Res.*, 102(B3), 5109-5110.

Allinson, C.R., Clarke, P.J., Edwards, S.J., King, M.A., Baker, T.F. & Cruddace, P.R., 2004. Stability of direct GPS estimates of ocean tide loading, *Geophys. Res. Lett.*, 31, L15603, doi:1029/2004GL020588.

Altamimi, Z., Sillard, P. & Boucher, C., 2002. ITRF2000: a new release of the International Terrestrial Reference Frame for Earth science applications, *J. geophys. Res.*, 107 (B10), 2214, doi:10.1029/2001JB000561.

Andersen, O.B., 1999. Shallow-water tides in the northwest European shelf region from TOPES/POSEIDON altimetry, *J. geophys. Res.*, 104(C4), 7729-7741.

Andersen, O.B., Woodworth, P.L. & Flather, R.A., 1995. Intercomparison of recent ocean tide models, *J. geophys. Res.*, 100(C12), 25261-25282.

Andersen, O.B., Egbert, G.D., Erofeeva, S.Y. & Ray, R.D., 2006. Mapping non linear shallow-water tides: a look at the past and future, *Ocean Dynamics*, 56, 416-429, doi:10.1007/s10236-006-0060-7.

Baker, T.F., Curtis, D.J. & Dodson, A.H., 1995. Ocean Tide Loading and GPS, *GPS World*, 54-59.

Baker, T.F. & Bos, M.S., 2003. Validating Earth and ocean tide models using tidal gravity measurements, *Geophys. J. Int.*, 152, 468-485.

Blewitt, G., 1989. Carrier phase ambiguity resolution for the global positioning system applied to geodetic beselines up to 2000 km, *J. geophys. Res.*, 98, 10187-10203.

Blewitt, G., Lavallée, D., Clarke, P. & Nurutdinov, K., 2001. A new global mode of Earth deformation : Seasonal cycle detected, *Science*, 294, 2342-2345.

Boy, J.-P., Llubbes, M., Ray, R., Hinderer, J., Florsch, N., Rosat, S., Lyard, F. & Letellier, T., 2004. Non-linear oceanic tides observed by superconducting gravimeters in Europe, *J. of Geodyn.*, 38 391-405, doi:10.1016/j.jog.2004.07.017.

Dong, D., Fang, P., Bock, Y., Cheng, M.K. & Miyazaki, S., 2002. Anatomy of apparent seasonal variations from GPS-derived site position time series, *J. geophys. Res.*, 107(B4), doi:1029/2001JB000573.

Dragert, F., James, T.S. & Lambert, A., 2000. Ocean loading corrections for continuous GPS: A case study at the Canadian coastal site Holberg, *Geophys. Res. Lett.*, 27, 2045-2048.

Duan, J., Bevis, M., Fang, P., Bock, Y., Chiswell, S., Businger, S., Rocken, C., Solheim, F., VanHove, T., Ware, R.H., McClusky, Herring, T.A. & King, R.W., 1996. GPS meteorology: Direct estimation of the absolute value of precipitable water, *J. Appl. Meteorol.*, 35, 830–838.

Efron, B. & Tibshirani, R.J., 1993. *An Introduction to the Bootstrap*, vol. 57 Monographs on Statistics and Applied Probability, 436 pp, Chapman & Hall, New-York.

Farrell, W.E., 1972. Deformation of the Earth by surface loads, *Rev. of Geophysics and Space Physics*, 10(3), 761-797.

Ferland, R., 2003. IGSMail 4748, 4758 and 4666, available at http://igscb.jpl.nasa.gov/mail/igsmail/2003/maillist.html.

Herring, T.A., 2003. *GLOBK: Global Kalman filter VLBI and GPS analysis program Version 10.1*. Internal Memorandum, Massachusetts Institute of Technology, Cambridge.

Herring, T.A., Davis, J.L. & Shapiro, I.I., 1990. Geodesy by radio interferometry: the application of Kalman filtering to the analysis of Very Long Baseline Infererometry data, *J. geophys. Res.*, 95, 12561-12581.

Hugentobler, U., Dach, R., Fridez, P. & Meindl, M, 2006. *Bernese GPS Software, Version 5.0 Draft*, Astronomical Institute, University of Bern.

Khan, S.A. & C.G. Tscherning, 2001. Determination of semi-diurnal ocean tide loading constituents using GPS in Alaska, *Geophys. Res. Lett.*, 28(11), 2249-2252.

Khan, S.A. & Scherneck, H.-G., 2003. The M2 ocean tide loading wave in Alaska: vertical and horizontal displacements, modelled and observed, *J. Geodesy*, 77, 117-127.

Khan, S. A., J. L. Høyer, 2004, Shallow-water loading tides in Japan from superconducting gravimetry, *J. Geodesy*, 78(4-5), doi:10.1007/s00190-003-0391-4.

King, M. & Aoki, S., 2003. Tidal observations on floating ice using a single GPS receiver, *Geophys. Res. Lett.*, 30 (3), 1138, doi:10.1029/2002GL016182.

King, M., Coleman, R. & Nguyen, L.N., 2003. Spurious periodic horizontal signals in sub-daily GPS position estimates, *J. Geodesy*, 77 (1-2), 15-21, doi:10.1007/s00190-002-0308-z.

King, M., Penna, N., Clarke, P. & King, E., 2005. Validation of ocean tide models around Antarctica using onshore GPS and gravity data, *J. Geophys. Res.*, 110 (B08401), doi:10.1029/2004JB003390.

King, R.W. & Bock, Y., 2005. *Documentation for GAMIT GPS analysis software, Release 10.2,* Massachusetts Institute of Technology, Cambridge.

Lefèvre, F., Lyard, F., Le Provost, C. & Schrama, E.J. O., 2002. FES99 : A global tide finite element solution assimilating tide gauge and altimetric information, *J. Atmos. Oceanog. Tech.*, 19, 1345-1356.

Llubes M., Florsch, N., Amalvict, M., Hinderer, J., Lalancette, M.-F., Orseau, D. & Simon, B., 2001. Observation gravimétriques des surcharges océaniques : premières expériences en Bretagne, *C.R. Académie Sciences*, Series IIa, 332, 77-82.

Llubes, M., Florsch, N., Boy, J.-P., Amalvict, M., Bonnefond, P., Bouin, M.-N., Durand, S., Esnoult, M.-F., Exertier, P., Hinderer, J., Lalancette, M.-F., Masson, F., Morel, L., Nicolas, J., Vergnolle, M. & Woppelmann, G, in revision 2007. A multi-technique monitoring of ocean loading in North of France, *C.R. Académie Sciences*.

Lyard F., Lefevre F., Letellier T. & Francis O., 2006. Modelling the global ocean tides: A modern insight from FES2004, *Ocean Dynamics*, 56, 394-415.

McCarthy, D.D. & Petit, G, 2004. IERS Conventions (2003). (IERS Technical Note ; 32) Frankfurt am Main: Verlag des Bundesamts für Kartographie und Geodäsie, 2004. 127 pp., paperback, ISBN 3-89888-884-3.

Melachroinos, S.A., Biancale, R., Llubes, M., Perosanz, F., Lyard, F., Vergnolle, M., Bouin, M.-N., Masson, F., Nicolas, J., Morel, L. & Durand, S., 2007. Ocean tide loading (OTL) displacements from global and local grids: Comparisons to GPS estimates over the shelf of Brittany, France, *J. Geodesy*, doi:10.1007/s00190-007-0185-6.

Melbourne, W.G., 1985. The case for ranging in GPS-based geodetic system, in Goad CC (ed) *First International Symposium on Precise Positioning with GPS*, pp. 373-386, Goad CC (ed), US Department of Commerce, Rockville, MD.

Niell, A.E., 1996. Global mapping functions for the atmosphere delay at radio wavelengths, *J. geophys. Res.*, 101, 3227-3246.

Pawlowicz, R., Beardsley, B. & Lentz, S, 2002. Classical tidal harmonic analysis including error estimates in MATLAB using T-TIDE, *Computers and Geosciences*, 28(8), 929-937.

Penna, N.T. & Stewart, M.P., 2003. Aliased tidal signatures in continuous GPS height time series, *Geophys. Res. Lett.*, 30(23), 2184, doi:10.1029/2003GL018828.

Penna, N.T., King, M.A. & Stewart, M.P., 2007. GPS height time series: Short period origins of spurious long period signals, *J. geophys. Res.*, 112, B02402, doi:10.1029/2005JB004047.

Ragheb, A.E., Clarke, P.J. & Edwards S.J., 2007. GPS sidereal filtering : coordinate- and carrier-phase-level strategies, *J. Geodesy*, 81, 325-335, doi:10.1007/s00190-006-0113-1.

Ray, R.D., 1999. *A global ocean tide model from TOPEX/Poseidon altimetry: GOT99.2*, NASA Tech. Memo., 209478, 58 pp.

Rothacher, M., Beutler, G., Weber, R. & Hefty, J., 2001. High-frequency variation of Earth rotation from global positioning system data, *J. geophys. Res.*, 106(B7), 13711-13738.

Saastamoinen, J., 1972. Atmospheric correction for the troposphere and stratosphere in radio ranging of satellite, Geophysical Monograph 15, The use of artificial satellites for geodesy, American Geophysical Union, Washington D.C..

Scherneck, H-G., Johansson, J.M. & Webb, F.H., 2000. Ocean loading tides in GPS and rapid variations of the frame origin, in *Geodesy beyond 2000: The challenges of the first decade*, pp 32-40, Schwarz K-P (ed), IAG General Assembly, Birmingham, 19-30 July.

Shum, C.K., Woodworth, P.L., Andersen, O.B., Egbert, G.D., Francis, O., King, C., Klosko, S.M., Le Provost, C., Li, X. Molines, J.-M., Parke, M.E., Ray, R.D., Schlax, M.G., Stammer, D., Tierney, C.C., Vincent, P. & Wunsch, C.I., 1997. Accuracy assessment of recent ocean tide models, *J. geophys. Res.*, 102(C11), 25173-25194.

Thomas, I.D., King, M.A. & Clarke, P.J., 2007. A comparison of GPS, VLBI and model estimates of ocean tide loading displacements, *J. Geod.*, 81, 359-368, doi:10.1007/s00190-006-0118-9.

Tregoning P., Boers, R. & O'Brien, D., 1998. Accuracy of absolute precipitable water vapor estimates from GPS observations, *J. geophys. Res.*, 103(D22), 28,701-28,710.

van Dam, T., Whar, J., Milly, P.C.D., Shmakin, A.B., Blewitt, G., Lavallée, D. & Larson, K.M., 2001. Crustal displacements due to continental water loading, *Geophys. Res. Lett.*, 28(4), 651-654.

Vey, S., Calais, E., Llubes, M., Florsch, N., Wöppelmann, G., Hinderer, J., Amalvict, M., Lalancette, M.F., Simon, B., Duquenne, F. & Haase, J.S., 2002. GPS Measurements of Ocean Loading and its Impact on Zenith Tropospheric Delay Estimates: A Case Study in Brittany, France, *J. Geodesy*, 76(8), 419-427.

Zumberge, J.F., Heflin, M.B., Jefferson, D.C., Watkins, M.M. & Webb, F.H., 1997. Precise Point Positioning for the efficient and robust analysis of GPS data from large networks, *J. geophys. Res.*, 102 (B3), 5005-5017.

Wessel, P., and W. H. F. Smith, 1998. New improved version of the Generic Mapping Tools Released, *EOS Trans. AGU, 79*, 579. http://gmt.soest.hawaii.edu/

Figure legends

Figure 1: Amplitude of the M2 tidal load on the vertical component in the Brittany-Cotentin region derived from FES2004 ocean tide model of Lyard et al. (2006). Values are in mm. The GPS stations used in this work are displayed with their name. BRST, RENN, and MANS (black symbol) belong to the French Permanent Network (RGP). The other stations (white symbol) are campaign stations deployed during the 2004 French Ocean Tide Loading campaign.

Figure 2: St1, St2, and predicted position time series (in mm) for the north, east, and up components at Cherbourg (CHER, Fig. 1) over 20 days extracted from the complete 105-day position time series (for clarity purposes). The St1 and St2 observed position time series (black) are represented along with the predicted position time series derived from FES2004 OT model (grey), on the top and bottom of each subplot respectively. The abbreviations used are: St1 for St1 observed solution, St2 for St2 observed solution, mod for model, and wsdd for Weighted Standard Deviation of the Difference.

Figure 3: Amplitude spectra (in mm) at Cherbourg (CHER) on the north, east, and up components based on the St1 (grey, on the left), St2 (grey, on the right), and predicted (FES2004, black) time series. The abbreviation std. dev. is for standard deviation (in mm).

Figure 4: Phasor diagrams (in mm) at Cherbourg (CHER, black) and Brest (BRST, grey) on the north (top), east (middle), and up (bottom) components for the semi-diurnal (M2, S2, N2) and diurnal (K1, O1, Q1) constituents of the ocean tide loading displacement signal. The GPS estimates from St1 and St2 are represented by square and circle, respectively, along with their amplitude error ellipse at 95% confidence level. The predicted estimates from FES2004 are represented by the cross. Scales of the phasor diagrams are optimized for each constituent. They are equal on the north and east components but different with the vertical component.

Figure 5: Misfits (in mm) between solutions two by two based on the 3D estimations of M2 constituent (black), and on the 3D estimations of all the 6 considered constituents (grey) at each station. Misfits between St1 and St2 estimations are displayed on the top, between St1 estimations and predictions on the middle, and between St2 estimations and predictions on the bottom. Abbreviations are explained in Fig. 2.

Figure 6: Amplitude spectra (in mm) at MALO (top), DUCE (middle), and COUT (bottom) on the vertical component based on the St1 (grey, on the left), St2 (grey, on the right), and predicted (FES2004, black) time series. The abbreviation std. dev. is for standard deviation (in mm).

Tables

Table 1: Weighted standard deviation of the differences between the St1 and St2 observed solutions (St1, St2) and the predicted solution (Mod) at each of the 14 stations of our network (in mm) on the north, east, and up components (N, E, U).

	St1/St2			St1/Mod			St2/Mod		
	N	E	U	N	E	U	N	E	U
BAYE	3.2	4.4	8.8	5.0	4.5	11.2	3.3	3.3	9.1
BRST	4.0	4.7	11.2	6.0	4.6	14.6	4.0	3.7	12.1
CHER	3.3	4.1	8.3	5.3	4.2	11.9	3.5	3.2	9.6
COUT	3.0	3.7	8.2	4.8	3.8	11.6	3.5	3.4	9.3
DIBE	3.2	3.9	9.6	5.3	3.7	13.0	3.9	3.5	11.4
DUCE	3.0	3.6	8.2	4.8	3.8	11.1	3.5	3.3	9.4
LAMB	3.1	4.2	8.8	5.0	4.3	12.4	3.7	3.8	11.0
MALO	3.2	3.8	8.6	5.2	4.0	12.2	3.8	3.6	10.6
MANS	3.7	4.1	10.3	5.6	4.2	13.4	3.8	3.4	10.8
PAIM	3.3	4.0	9.2	5.7	4.1	13.6	3.8	3.5	10.6
RENN	3.6	3.9	9.6	5.6	4.1	13.1	3.9	3.4	10.0
SURZ	3.3	4.0	9.5	4.4	3.7	12.0	3.3	3.4	10.2
TREV	3.9	4.4	11.7	5.5	4.0	16.7	3.6	3.8	12.1
YGEA	3.3	4.0	9.5	4.7	4.1	11.9	3.5	3.6	9.9

Table 2: Amplitudes (in mm) of the 6 main tidal components (semi diurnal and diurnal) for the north, east, and up components on the 14 stations of our network as estimated from the St1 and St2 analysis and predicted from the FES2004 model. The sigmas (italic values) are at 95% level confidence.

Site	k	M2			S2			N2			K1			O1			Q1		
		St1	St2	Mod	St1	St2	Mod	St1	St2	Mod	St1	St2	Mod	St1	St2	Mod	St1	St2	Mod
BRST	U	41.8	41.2	39.4	14.2	12.6	14.1	7.9	8.5	8.1	0.4	1.3	1.3	3.2	3.6	3.5	0.8	1.0	1.0
		1.9	*1.1*		*1.6*	*1.0*		*1.8*	*1.1*		*1.9*	*1.5*		*2.5*	*1.3*		*1.8*	*1.3*	
	N	7.8	7.7	6.9	3.8	3.9	2.8	1.3	1.4	1.5	3.1	3.3	3.5	2.9	3.0	2.9	0.9	0.9	0.6
		0.7	*0.5*		*0.6*	*0.5*		*0.6*	*0.5*		*0.7*	*0.5*		*0.6*	*0.5*		*0.7*	*0.5*	
	E	7.8	7.7	8.3	2.8	3.6	2.8	2.2	2.0	1.9	3.9	3.9	2.8	2.2	1.7	1.8	0.6	0.3	0.4
		1.1	*0.6*		*0.9*	*0.6*		*0.9*	*0.6*		*1.1*	*0.7*		*1.0*	*0.6*		*0.9*	*0.6*	
TREV	U	35.2	36.1	36.6	16.6	14.5	13.1	8.0	8.1	7.6	4.7	1.3	1.3	1.8	3.1	3.4	1.3	1.6	1.0
		1.2	*0.6*		*1.2*	*0.7*		*1.2*	*0.6*		*0.7*	*0.7*		*0.8*	*0.7*		*0.8*	*0.7*	
	N	8.1	7.8	7.2	3.0	3.6	2.8	1.4	1.6	1.5	3.7	3.2	3.5	2.8	2.9	2.9	0.8	0.9	0.6
		0.3	*0.3*		*0.4*	*0.3*		*0.3*	*0.3*		*0.3*	*0.2*		*0.3*	*0.2*		*0.3*	*0.2*	
	E	7.8	8.1	8.1	2.9	3.3	2.7	1.7	2.0	1.8	3.4	4.4	2.8	2.0	1.5	1.8	0.2	0.3	0.4
		0.4	*0.3*		*0.4*	*0.3*		*0.4*	*0.3*		*0.4*	*0.2*		*0.5*	*0.2*		*0.3*	*0.2*	
DIBE	U	39.2	40.0	39.4	17.1	15.7	14.2	8.1	8.3	8.0	3.2	2.4	1.2	2.6	3.9	3.4	1.2	1.2	1.0
		1.7	*1.4*		*1.7*	*1.4*		*1.7*	*1.3*		*1.3*	*1.2*		*1.3*	*1.2*		*1.2*	*1.2*	
	N	8.4	8.3	7.2	3.4	3.8	3.1	1.4	1.4	1.5	3.5	3.8	3.6	2.4	2.5	2.9	0.6	0.7	0.6
		0.5	*0.6*		*0.5*	*0.6*		*0.6*	*0.7*		*0.5*	*0.4*		*0.5*	*0.4*		*0.5*	*0.4*	
	E	8.5	8.6	8.7	2.9	4.0	3.0	2.1	2.1	2.0	3.8	4.6	2.8	1.9	1.6	1.8	0.4	0.1	0.4
		0.9	*0.7*		*0.8*	*0.7*		*0.9*	*0.7*		*0.6*	*0.4*		*0.6*	*0.5*		*0.5*	*0.3*	
YGEA	U	27.8	28.0	27.9	10.7	9.0	9.7	5.4	5.8	5.7	2.0	2.0	0.9	3.1	3.6	3.0	1.4	1.3	0.9
		1.2	*1.1*		*1.1*	*1.0*		*1.0*	*0.9*		*1.3*	*1.1*		*1.3*	*1.1*		*1.3*	*1.0*	
	N	7.5	7.7	7.0	3.0	3.3	2.9	1.5	1.6	1.5	3.8	3.7	3.6	2.2	2.4	2.9	0.8	0.8	0.6
		0.5	*0.5*		*0.5*	*0.5*		*0.5*	*0.5*		*0.7*	*0.6*		*0.6*	*0.5*		*0.6*	*0.5*	
	E	8.0	7.8	8.4	3.3	3.9	2.8	1.7	1.8	1.9	3.5	4.4	2.8	1.9	1.7	1.8	0.3	0.5	0.4
		0.7	*0.5*		*0.7*	*0.5*		*0.7*	*0.5*		*0.8*	*0.5*		*1.0*	*0.6*		*0.8*	*0.5*	
PAIM	U	35.2	35.4	34.6	15.1	14.6	12.2	6.9	7.3	6.9	2.0	2.6	1.0	2.7	3.9	3.2	1.2	1.2	0.9
		1.7	*1.1*		*1.9*	*1.2*		*1.7*	*1.1*		*1.1*	*1.2*		*1.2*	*1.1*		*1.1*	*1.0*	
	N	8.1	8.2	7.4	3.1	3.4	3.1	1.6	1.6	1.5	4.0	3.8	3.6	2.5	2.7	2.9	0.5	0.6	0.6
		0.7	*0.5*		*0.7*	*0.5*		*0.7*	*0.6*		*0.5*	*0.4*		*0.4*	*0.4*		*0.4*	*0.4*	
	E	8.5	8.0	8.4	3.3	3.8	2.9	1.9	2.1	1.9	3.1	4.5	2.7	2.0	1.8	1.8	0.8	0.4	0.3
		0.6	*0.5*		*0.5*	*0.5*		*0.6*	*0.6*		*0.7*	*0.4*		*0.7*	*0.4*		*0.7*	*0.4*	
SURZ	U	25.8	27.2	28.8	10.1	8.5	10.2	6.5	7.4	6.0	1.4	0.1	1.0	2.9	4.2	3.1	0.8	0.6	0.9
		0.3	*0.6*		*0.3*	*0.6*		*0.3*	*0.6*		*0.7*	*0.3*		*0.7*	*0.5*		*0.6*	*0.5*	
	N	7.3	7.1	6.7	2.8	2.9	2.5	1.7	1.8	1.4	3.8	3.6	3.5	2.4	2.8	2.9	0.6	0.6	0.6
		0.1	*0.1*		*0.1*	*0.1*		*0.1*	*0.1*		*0.2*	*0.1*		*0.1*	*0.1*		*0.2*	*0.1*	
	E	*7.8*	8.1	8.8	3.1	3.6	2.8	2.1	1.9	2.0	4.1	4.8	2.8	1.7	1.7	1.8	1.0	0.8	0.4
		0.3	*0.2*		*0.3*	*0.2*		*0.3*	*0.2*		*0.3*	*0.1*		*0.3*	*0.1*		*0.2*	*0.1*	
LAMB	U	26.8	27.2	26.4	8.6	8.1	9.0	5.6	6.0	5.3	2.8	2.4	0.8	2.1	3.1	2.9	1.3	1.4	0.8
		1.0	*0.9*		*1.0*	*0.9*		*1.2*	*1.0*		*1.3*	*1.1*		*1.0*	*0.9*		*1.2*	*1.0*	
	N	8.2	8.3	7.6	3.0	3.3	3.2	1.9	1.8	1.6	3.8	3.8	3.6	2.5	2.7	2.9	0.9	0.8	0.6
		0.5	*0.5*		*0.5*	*0.5*		*0.5*	*0.6*		*0.5*	*0.4*		*0.6*	*0.4*		*0.5*	*0.4*	
	E	7.9	7.9	8.7	2.3	3.4	2.8	1.6	1.7	1.9	3.1	4.0	2.8	1.8	1.9	1.8	0.5	0.6	0.4
		0.6	*0.6*		*0.5*	*0.5*		*0.5*	*0.5*		*0.6*	*0.5*		*0.7*	*0.5*		*0.6*	*0.4*	

Table 2 (continued)

Site	k	M2			S2			N2			K1			O1			Q1		
		St1	St2	Mod	St1	St2	Mod	St1	St2	Mod	St1	St2	Mod	St1	St2	Mod	St1	St2	Mod
MALO	U	27.3	28.1	28.4	9.2	8.5	9.6	5.9	6.4	5.5	3.5	2.1	0.8	2.3	3.1	2.9	1.4	1.4	0.9
		1.2	*0.9*		*1.1*	*0.8*		*1.2*	*0.9*		*1.0*	*1.1*		*1.2*	*1.3*		*1.3*	*1.3*	
	N	8.8	8.9	7.9	3.5	3.9	3.3	1.6	1.6	1.6	3.1	3.3	3.6	2.1	2.5	2.9	0.8	0.7	0.6
		0.6	*0.5*		*0.5*	*0.4*		*0.5*	*0.4*		*0.6*	*0.5*		*0.6*	*0.5*		*0.6*	*0.5*	
	E	8.6	8.8	9.3	2.9	3.7	2.9	1.9	1.9	2.0	3.6	4.4	2.8	2.3	1.9	1.8	0.8	0.6	0.4
		0.8	*0.5*		*0.8*	*0.5*		*0.8*	*0.5*		*0.9*	*0.6*		*0.7*	*0.5*		*0.7*	*0.5*	
RENN	U	19.0	18.6	19.6	7.7	6.8	6.7	4.0	4.2	4.1	1.0	0.4	0.6	1.5	2.4	2.6	0.9	1.1	0.7
		1.4	*1.1*		*1.4*	*1.3*		*1.5*	*1.2*		*1.2*	*0.7*		*1.4*	*0.9*		*1.1*	*0.9*	
	N	6.1	6.4	6.0	2.5	3.0	2.2	1.5	1.4	1.3	2.7	3.0	3.6	2.6	2.8	2.9	0.5	0.5	0.6
		0.6	*0.4*		*0.6*	*0.4*		*0.6*	*0.5*		*0.6*	*0.5*		*0.6*	*0.5*		*0.6*	*0.5*	
	E	7.1	7.3	8.2	2.4	2.6	2.5	1.4	1.8	1.8	3.2	3.8	2.7	2.1	2.1	1.8	0.2	0.4	0.4
		0.8	*0.5*		*0.8*	*0.5*		*0.8*	*0.6*		*0.8*	*0.5*		*0.7*	*0.6*		*0.6*	*0.4*	
CHER	U	18.6	18.6	17.8	7.2	7.2	6.2	2.9	3.7	3.6	2.8	1.5	0.7	1.7	2.7	2.8	1.3	1.3	0.9
		1.3	*0.9*		*1.5*	*1.0*		*1.7*	*1.0*		*1.3*	*1.0*		*1.4*	*1.1*		*1.1*	*1.2*	
	N	6.2	6.1	5.8	2.1	1.8	1.7	1.5	1.4	1.3	3.2	3.4	3.5	2.3	2.6	2.9	1.0	0.9	0.6
		0.5	*0.4*		*0.5*	*0.4*		*0.4*	*0.4*		*0.6*	*0.5*		*0.6*	*0.5*		*0.6*	*0.5*	
	E	10.8	10.7	11.0	3.9	3.8	3.5	2.0	2.3	2.2	2.9	4.2	2.7	2.5	2.1	1.8	1.5	0.8	0.4
		0.8	*0.5*		*0.7*	*0.5*		*0.8*	*0.5*		*0.8*	*0.4*		*0.9*	*0.5*		*0.9*	*0.5*	
COUT	U	19.3	19.5	19.1	8.8	7.9	6.3	3.8	4.0	3.8	3.8	2.9	0.6	1.9	2.8	2.7	1.2	1.2	0.8
		1.6	*1.2*		*1.5*	*1.1*		*1.6*	*1.3*		*1.2*	*1.2*		*1.4*	*1.2*		*1.3*	*1.2*	
	N	5.8	6.0	5.7	1.9	1.9	1.8	1.3	1.2	1.2	3.3	3.5	3.6	2.3	2.6	2.9	0.6	0.7	0.6
		0.5	*0.5*		*0.5*	*0.5*		*0.5*	*0.4*		*0.5*	*0.4*		*0.5*	*0.4*		*0.5*	*0.4*	
	E	10.0	10.1	10.7	2.4	3.3	3.4	2.4	2.4	2.2	3.8	4.3	2.8	2.2	2.0	1.8	0.7	0.5	0.4
		0.6	*0.6*		*0.6*	*0.5*		*0.6*	*0.5*		*0.7*	*0.5*		*0.6*	*0.4*		*0.6*	*0.4*	
DUCE	U	16.9	17.2	17.7	6.8	6.4	5.8	3.6	3.8	3.6	1.8	1.0	0.5	2.5	2.6	2.6	1.6	1.3	0.7
		1.3	*1.0*		*1.3*	*1.0*		*1.2*	*0.9*		*1.2*	*1.0*		*1.1*	*0.9*		*1.2*	*0.9*	
	N	6.1	6.3	5.9	2.4	2.6	2.1	1.3	1.2	1.3	3.4	3.5	3.6	2.3	2.7	2.9	0.7	0.7	0.6
		0.5	*0.4*		*0.5*	*0.4*		*0.5*	*0.4*		*0.7*	*0.5*		*0.6*	*0.5*		*0.7*	*0.4*	
	E	8.5	8.3	9.1	2.1	2.9	2.7	1.7	1.9	1.9	3.3	4.4	2.7	2.3	2.0	1.8	0.9	0.7	0.4
		0.6	*0.6*		*0.6*	*0.5*		*0.6*	*0.6*		*0.7*	*0.4*		*0.6*	*0.4*		*0.6*	*0.3*	
BAYE	U	8.6	8.4	8.2	4.0	3.0	2.4	1.4	1.8	1.8	1.0	0.8	0.4	1.9	2.7	2.5	0.6	0.8	0.7
		1.4	*0.8*		*1.2*	*0.8*		*1.2*	*0.8*		*1.3*	*0.9*		*1.2*	*0.8*		*1.0*	*0.8*	
	N	7.1	7.2	6.9	2.3	2.2	2.1	1.6	1.5	1.4	3.4	3.5	3.6	2.2	2.6	2.9	1.0	0.8	0.6
		0.5	*0.4*		*0.5*	*0.4*		*0.5*	*0.3*		*0.5*	*0.3*		*0.5*	*0.3*		*0.5*	*0.3*	
	E	7.6	7.9	8.7	2.4	2.8	2.6	1.9	1.9	1.8	4.3	4.3	2.7	1.9	1.8	1.8	1.0	0.5	0.4
		0.9	*0.5*		*0.9*	*0.5*		*0.7*	*0.4*		*1.0*	*0.5*		*1.0*	*0.5*		*0.8*	*0.5*	
MANS	U	12.1	11.8	12.5	5.8	4.1	4.4	3.0	3.1	2.7	3.6	3.4	0.7	1.9	2.2	2.3	0.3	0.7	0.6
		1.3	*0.9*		*1.3*	*0.9*		*1.3*	*0.9*		*1.4*	*0.9*		*1.4*	*0.9*		*1.0*	*0.7*	
	N	4.1	4.3	4.1	1.5	1.7	1.2	0.8	0.9	0.9	3.3	3.4	3.6	2.3	2.7	2.9	0.5	0.6	0.6
		0.7	*0.4*		*0.7*	*0.4*		*0.7*	*0.4*		*0.7*	*0.5*		*0.7*	*0.5*		*0.6*	*0.4*	
	E	5.1	5.3	6.1	2.4	2.4	1.7	1.7	1.5	1.3	2.7	3.4	2.6	2.2	1.8	1.7	0.5	0.6	0.3
		1.2	*0.7*		*1.1*	*0.6*		*1.2*	*0.7*		*1.0*	*0.7*		*1.1*	*0.7*		*0.9*	*0.7*	

Table 3: Phases (in degree) of the 6 main tidal components (semi diurnal and diurnal) for the north, east, and up components on the 14 stations of our network as estimated from the St1 and St2 analysis and predicted from the FES2004 model. The sigmas (italic values) are at 95% level confidence.

Site	k	M2			S2			N2			K1			O1			Q1		
		St1	St2	Mod	St1	St2	Mod	St1	St2	Mod	St1	St2	Mod	St1	St2	Mod	St1	St2	Mod
BRST	U	106.5	105.8	103.4	334.1	343.8	327.7	305.7	305.4	307.9	69.3	342.4	299.6	247.8	243.9	249.3	88.5	94.4	84.0
		2.2	*1.3*		*8.2*	*5.5*		*12.3*	*6.8*		*201.9*	*58.4*		*48.7*	*25.4*		*138.1*	*74.6*	
	N	22.1	25.7	31.4	249.6	245.2	245.3	250.6	249.2	244.0	139.1	133.3	138.6	170.2	172.5	174.9	21.8	31.4	21.3
		5.3	*4.5*		*10.4*	*8.1*		*24.0*	*18.9*		*12.3*	*8.7*		*13.3*	*9.1*		*49.9*	*35.8*	
	E	86.6	84.1	88.9	291.3	289.3	305.3	285.1	292.3	293.6	272.3	294.8	297.2	310.1	307.1	307.9	165.9	126.0	137.7
		8.1	*4.8*		*20.6*	*9.2*		*24.7*	*16.3*		*17.1*	*10.1*		*31.0*	*23.8*		*104.9*	*106.5*	
TREV	U	101.0	98.9	95.7	330.6	335.2	317.6	298.9	300.8	300.3	56.7	353.0	291.0	255.3	250.4	247.8	113.8	106.3	82.2
		2.1	*1.0*		*4.0*	*2.2*		*8.7*	*4.2*		*11.1*	*25.6*		*24.6*	*11.9*		*39.4*	*26.9*	
	N	31.9	35.6	41.3	258.4	255.6	255.8	233.5	242.1	253.2	158.4	143.9	138.4	179.2	180.9	176.2	7.2	31.7	23.0
		2.3	*2.2*		*6.2*	*4.5*		*14.1*	*11.3*		*4.9*	*4.2*		*5.9*	*4.3*		*21.2*	*13.1*	
	E	86.9	83.5	90.5	307.5	300.4	307.2	283.4	287.8	295.1	294.7	295.3	297.3	302.9	300.4	307.2	268.8	152.4	136.2
		2.6	*2.0*		*7.0*	*4.9*		*13.5*	*8.8*		*8.2*	*2.4*		*11.2*	*7.1*		*153.4*	*37.2*	
DIBE	U	118.4	117.3	113.4	352.1	359.6	341.6	321.3	318.1	318.4	39.7	329.4	303.4	256.2	254.4	250.1	124.4	113.3	87.1
		2.4	*1.9*		*5.4*	*4.2*		*11.3*	*8.1*		*20.1*	*30.6*		*27.8*	*18.3*		*61.9*	*56.0*	
	N	8.3	9.7	18.3	240.5	232.2	235.6	226.7	227.1	232.0	133.1	125.9	138.2	173.5	170.5	172.8	10.5	27.2	18.3
		3.9	*4.3*		*11.2*	*11.2*		*21.9*	*25.6*		*8.3*	*5.9*		*11.0*	*8.1*		*48.4*	*30.5*	
	E	92.5	89.8	91.0	296.4	299.3	309.4	284.4	287.0	295.7	285.9	293.5	297.6	298.4	297.7	308.5	86.3	104.5	138.0
		4.7	*3.9*		*13.9*	*8.3*		*18.2*	*15.0*		*8.7*	*5.2*		*18.4*	*15.2*		*80.5*	*176.5*	
YGEA	U	111.1	110.5	106.2	336.0	342.4	331.3	310.1	310.2	310.8	89.5	26.7	285.8	244.1	242.1	248.3	91.6	99.0	86.7
		2.4	*2.2*		*5.3*	*6.0*		*10.7*	*9.5*		*37.6*	*32.7*		*25.3*	*19.2*		*63.0*	*50.5*	
	N	23.9	25.3	31.4	244.9	242.7	248.1	237.1	238.2	244.4	134.8	131.2	137.8	179.9	176.5	173.8	5.4	18.4	20.1
		4.4	*4.2*		*10.5*	*9.2*		*18.9*	*17.2*		*8.6*	*6.8*		*17.0*	*11.3*		*56.9*	*40.9*	
	E	90.0	88.9	94.1	309.6	302.1	313.2	292.7	293.4	298.6	290.7	293.4	298.0	307.2	307.1	308.0	116.6	147.7	138.0
		5.2	*3.9*		*12.0*	*8.2*		*23.1*	*15.9*		*15.1*	*6.8*		*27.1*	*18.2*		*119.5*	*61.9*	
PAIM	U	126.9	126.5	122.7	359.2	3.9	353.8	329.8	328.2	328.0	324.4	311.2	302.9	249.1	248.3	251.3	93.0	89.2	90.2
		2.7	*1.8*		*6.9*	*4.8*		*17.9*	*11.0*		*39.2*	*25.2*		*25.2*	*15.9*		*57.7*	*46.9*	
	N	12.1	15.1	23.5	248.1	236.9	241.7	234.7	233.3	236.8	135.6	134.0	137.8	171.0	170.8	172.3	14.2	25.2	17.6
		4.8	*3.8*		*13.5*	*9.1*		*26.9*	*17.9*		*6.7*	*5.3*		*10.7*	*8.7*		*52.5*	*35.8*	
	E	88.4	86.5	89.1	301.7	300.9	307.7	287.1	286.0	294.4	296.7	300.0	298.0	311.9	306.8	309.2	114.1	153.6	139.6
		3.8	*3.7*		*9.1*	*7.1*		*18.1*	*14.6*		*12.6*	*6.3*		*19.9*	*13.4*		*51.4*	*54.9*	
SURZ	U	100.8	99.6	95.8	328.0	339.4	318.0	307.3	306.3	301.0	37.7	49.6	278.1	245.5	241.9	247.1	70.6	48.0	84.1
		0.7	*1.1*		*1.7*	*3.5*		*2.7*	*4.4*		*29.7*	*228.3*		*14.2*	*7.2*		*59.8*	*54.6*	
	N	41.9	42.3	47.5	283.9	271.2	263.1	255.9	263.3	259.6	142.3	132.3	137.6	176.5	173.7	175.6	352.9	44.1	22.7
		1.1	*1.1*		*3.0*	*2.7*		*4.7*	*4.2*		*2.1*	*1.9*		*3.1*	*2.4*		*14.5*	*12.0*	
	E	83.7	90.0	94.3	312.4	306.1	313.0	272.3	278.1	298.7	297.4	300.1	298.2	337.3	309.8	306.4	129.7	162.7	134.6
		2.2	*1.4*		*5.3*	*3.3*		*7.1*	*5.6*		*3.3*	*1.4*		*9.2*	*4.6*		*15.2*	*9.1*	
LAMB	U	124.1	123.0	116.3	357.8	2.7	345.1	321.5	320.4	320.9	40.4	36.2	287.4	248.3	243.9	249.3	105.5	102.7	89.4
		2.3	*2.0*		*7.2*	*6.7*		*11.3*	*9.3*		*26.3*	*26.9*		*31.3*	*19.2*		*52.6*	*43.6*	
	N	19.7	19.6	25.5	246.1	238.7	245.6	241.1	238.5	239.2	144.2	136.2	137.6	180.8	174.2	172.5	9.4	13.9	17.6
		3.8	*3.4*		*10.4*	*8.6*		*15.8*	*15.7*		*8.3*	*5.5*		*12.9*	*7.8*		*35.1*	*26.3*	
	E	101.5	98.6	101.3	314.0	312.6	324.2	314.2	302.2	305.3	288.5	293.4	298.8	318.4	307.5	308.3	141.9	155.7	137.0
		4.2	*3.6*		*13.3*	*7.6*		*20.1*	*17.5*		*11.2*	*6.2*		*19.3*	*13.2*		*77.9*	*39.9*	

Table 3 continued

Site	k	M2			S2			N2			K1			O1			Q1		
		St1	St2	Mod	St1	St2	Mod	St1	St2	Mod	St1	St2	Mod	St1	St2	Mod	St1	St2	Mod
MALO	U	136.2	134.7	129.8	15.8	22.7	3.8	332.4	333.1	335.3	28.5	20.4	293.8	232.3	239.7	251.0	112.2	105.3	92.1
		2.7	*1.9*		*7.4*	*5.4*		*12.6*	*8.0*		*19.4*	*32.3*		*28.0*	*22.7*		*46.3*	*52.0*	
	N	21.4	20.8	26.5	247.2	238.3	248.2	238.2	236.4	240.3	138.4	130.0	137.4	176.1	170.5	171.8	352.6	10.2	16.7
		4.2	*3.2*		*9.8*	*7.2*		*20.5*	*15.9*		*11.5*	*8.8*		*16.9*	*11.6*		*43.7*	*43.1*	
	E	109.0	109.2	110.7	322.2	319.6	338.6	313.7	321.2	314.4	287.9	292.1	299.6	316.8	310.3	308.3	125.3	125.4	136.4
		5.1	*3.3*		*17.0*	*8.8*		*23.9*	*15.0*		*13.1*	*7.3*		*19.8*	*15.7*		*60.1*	*58.2*	
RENN	U	110.7	110.8	104.3	341.6	356.8	327.7	309.9	309.2	308.6	80.5	263.0	261.3	234.9	239.7	247.0	111.0	103.8	88.5
		4.3	*3.7*		*11.7*	*11.0*		*21.3*	*16.9*		*90.7*	*118.9*		*55.3*	*21.7*		*84.5*	*43.2*	
	N	34.2	34.9	40.6	275.5	258.7	256.7	260.2	252.1	253.5	146.7	132.7	137.1	180.3	175.5	173.3	309.9	3.7	19.8
		6.2	*4.3*		*13.1*	*8.8*		*22.8*	*18.0*		*13.1*	*9.7*		*13.8*	*10.5*		*81.6*	*64.4*	
	E	103.5	100.7	105.1	291.9	299.2	329.1	309.4	310.3	308.7	275.2	285.6	299.2	313.7	305.9	308.3	99.1	103.5	137.3
		6.4	*4.1*		*19.1*	*11.7*		*35.7*	*16.7*		*14.2*	*7.8*		*23.2*	*14.2*		*160.9*	*75.8*	
CHER	U	153.1	151.6	143.8	25.0	34.6	18.4	356.8	347.6	348.3	34.3	63.3	312.8	263.0	252.9	254.2	78.0	91.2	100.1
		4.6	*3.1*		*11.9*	*8.2*		*31.7*	*16.5*		*25.3*	*46.7*		*42.1*	*23.5*		*59.5*	*53.8*	
	N	70.5	70.6	78.4	321.2	309.9	298.2	286.0	282.5	286.0	130.5	123.9	136.2	170.1	167.3	173.7	356.3	11.1	20.4
		4.5	*4.0*		*11.1*	*13.5*		*17.5*	*18.2*		*9.8*	*7.5*		*14.5*	*10.3*		*35.1*	*34.1*	
	E	122.0	121.4	121.6	348.9	339.0	356.0	317.1	327.3	325.8	282.1	296.8	300.6	324.9	312.9	309.4	131.2	145.2	137.3
		4.1	*2.8*		*12.4*	*8.0*		*18.8*	*11.1*		*16.6*	*6.2*		*19.1*	*12.3*		*32.5*	*31.0*	
COUT	U	138.9	137.6	130.3	13.9	22.1	2.8	336.6	332.5	334.8	47.0	29.1	286.3	232.1	241.0	251.0	95.0	100.1	95.4
		4.4	*3.3*		*9.8*	*8.8*		*21.5*	*15.8*		*17.7*	*21.9*		*35.7*	*21.4*		*74.0*	*65.5*	
	N	60.8	59.9	65.0	283.9	270.5	281.3	277.2	273.7	274.1	136.1	132.4	136.6	174.4	170.6	173.2	11.2	16.6	19.4
		5.2	*4.3*		*16.4*	*13.9*		*25.4*	*23.6*		*9.4*	*6.8*		*14.3*	*9.1*		*47.1*	*33.5*	
	E	128.4	125.7	126.0	357.4	343.6	1.9	333.6	332.4	329.9	280.7	289.6	300.9	312.1	305.0	308.5	136.1	149.3	136.5
		3.2	*3.0*		*15.1*	*10.3*		*13.7*	*12.9*		*7.6*	*5.0*		*14.0*	*10.6*		*49.7*	*52.2*	
DUCE	U	125.1	123.8	116.7	4.7	15.3	344.5	326.9	320.3	320.8	36.4	16.5	264.6	237.4	240.9	248.6	75.1	90.5	92.4
		4.3	*3.1*		*11.4*	*8.9*		*21.4*	*14.3*		*39.9*	*69.4*		*27.1*	*23.4*		*47.7*	*47.6*	
	N	41.7	42.2	47.2	261.3	254.6	263.9	265.5	259.8	259.3	141.1	132.8	136.7	174.8	170.9	172.7	349.2	14.0	18.5
		5.1	*4.1*		*11.8*	*9.9*		*24.6*	*20.4*		*11.9*	*8.2*		*16.0*	*10.4*		*56.6*	*43.1*	
	E	118.9	117.2	119.2	332.1	324.7	351.8	319.8	321.2	322.5	283.6	292.1	300.4	313.3	307.2	308.9	136.2	151.3	137.2
		4.3	*3.6*		*19.0*	*11.8*		*23.3*	*18.0*		*11.8*	*5.8*		*17.2*	*12.8*		*41.2*	*38.7*	
BAYE	U	148.5	148.4	134.1	13.8	35.8	358.6	355.3	344.1	334.0	261.5	56.1	278.5	226.3	236.9	251.6	44.3	74.7	100.2
		8.4	*6.5*		*18.4*	*14.7*		*57.3*	*26.8*		*73.9*	*70.0*		*33.9*	*18.8*		*123.7*	*69.4*	
	N	74.0	72.1	76.8	304.1	296.3	300.4	289.3	284.4	284.5	121.5	124.2	136.5	171.6	167.7	172.6	15.8	17.2	18.1
		3.8	*2.7*		*12.4*	*9.7*		*17.3*	*14.2*		*7.7*	*4.9*		*12.7*	*6.9*		*29.0*	*23.8*	
	E	122.0	120.2	122.6	348.1	333.5	357.6	307.9	320.0	326.2	274.2	292.9	301.1	309.2	308.4	310.4	154.1	161.9	139.5
		6.3	*3.5*		*20.6*	*9.9*		*25.4*	*16.1*		*13.0*	*6.8*		*33.0*	*18.6*		*53.4*	*54.8*	
MANS	U	96.5	100.5	94.4	325.3	357.0	313.6	309.1	296.9	299.1	159.3	172.9	222.9	253.2	254.1	245.3	20.0	87.1	90.6
		6.3	*4.4*		*13.1*	*13.2*		*27.6*	*18.0*		*22.1*	*15.2*		*39.1*	*22.0*		*190.4*	*87.9*	
	N	57.5	54.6	57.9	299.1	276.2	271.5	253.6	258.4	270.1	148.9	138.0	135.8	161.1	165.2	173.0	26.6	30.0	20.3
		10.9	*6.0*		*29.3*	*14.9*		*47.5*	*23.7*		*12.6*	*8.7*		*17.6*	*10.6*		*75.5*	*46.1*	
	E	98.2	99.2	107.0	290.7	286.8	331.4	302.0	309.6	310.1	274.2	291.5	300.1	293.3	298.2	310.9	216.4	196.0	141.2
		13.2	*7.7*		*27.7*	*17.2*		*42.0*	*27.5*		*21.3*	*10.9*		*26.2*	*20.6*		*112.1*	*68.0*	

Table 4: Amplitudes and phases of the M4, S4, and SK3 shallow-water loading constituents for the up component, at MALO, DUCE, and COUT located in the Mont St Michel area, as observed from the St1 and St2 analysis, and amplitude and phase of the M4 non linear term for the up component as predicted from FES2004 (Mod). The sigmas (italic values) are at 95% level confidence.

Site	k	M4						S4				SK3			
		St1		St2		Mod		St1		St2		St1		St2	
		A (mm)	Φ (deg)	A (mm)	Φ (deg)	A (mm)	Φ (deg)	A (mm)	Φ (deg)	A (mm)	Φ (deg)	A (mm)	Φ (deg)	A (mm)	Φ (deg)
MALO	U	1.30	165.2	0.85	151.4	0.58	151.9	1.65	296	1.61	331	2.02	23	2.26	351
		(1.12)	*(57.5)*	*(0.76)*	*(59.5)*			*(1.13)*	*(44)*	*(0.93)*	*(33)*	*(1.14)*	*(31)*	*(0.73)*	*(24)*
DUCE	U	0.25	123.2	0.49	136.6	0.31	162.4	0.71	300	1.74	341	2.75	17	2.82	350
		(0.60)	*(169.1)*	*(0.69)*	*(79.3)*			*(0.86)*	*(75)*	*(0.83)*	*(26)*	*(1.08)*	*(21)*	*(0.89)*	*(15)*
COUT	U	0.82	189.8	0.60	180.3	0.62	161.3	0.93	346	1.41	353	1.03	32	1.65	355
		(1.03)	*(77.1)*	*(0.85)*	*(98.2)*			*(1.21)*	*(77)*	*(0.91)*	*(45)*	*(0.86)*	*(54)*	*(0.73)*	*(24)*

Figure 1

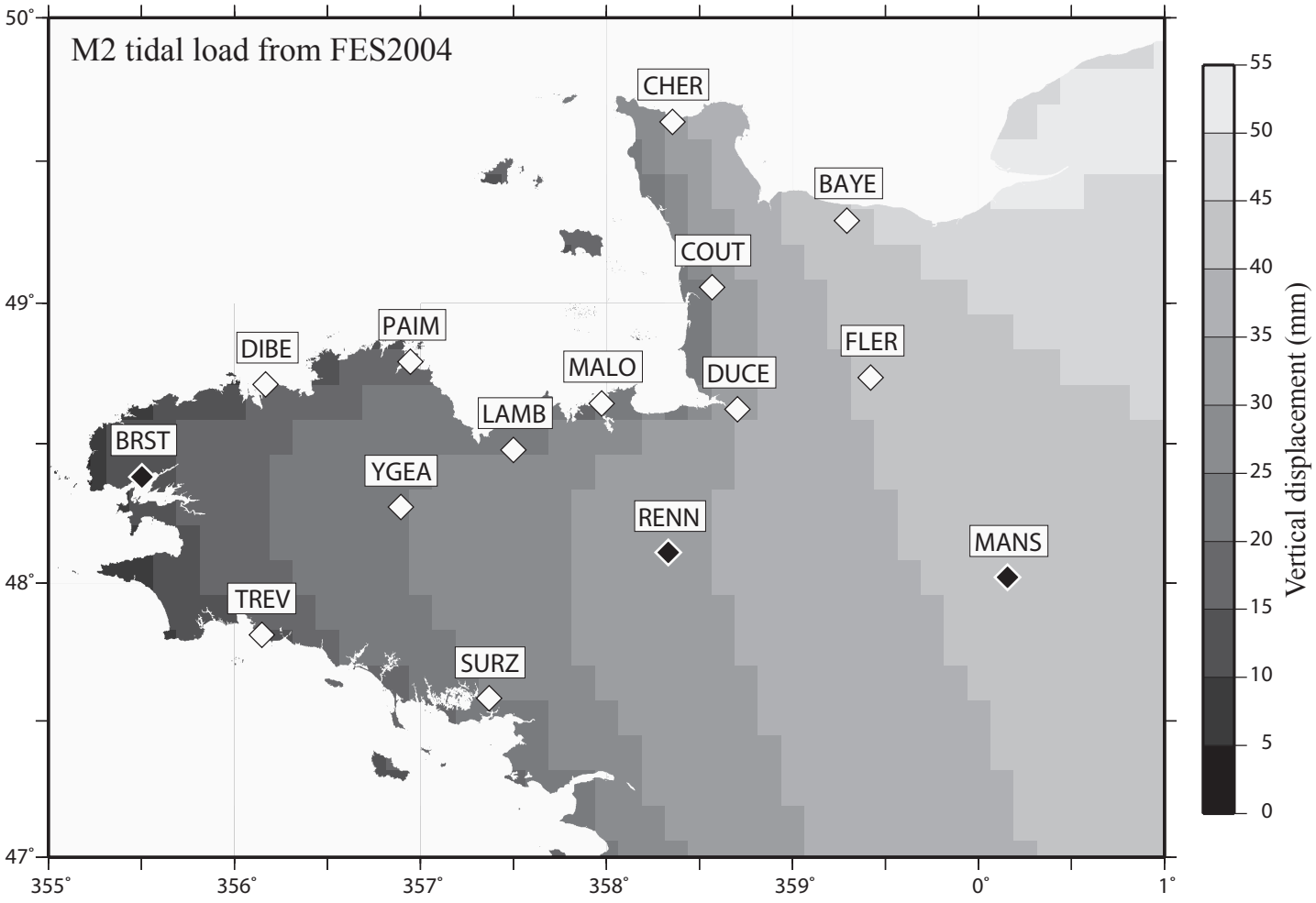
M2 tidal load from FES2004
CHER
BAYE
COUT
PAIM
DIBE
FLER
MALO
DUCE
LAMB
BRST
YGEA
RENN
MANS
TREV
SURZ
50°
49°
48°
47°
355°
356°
357°
358°
359°
0°
1°
Vertical displacement (mm)
55
50
45
40
35
30
25
20
15
10
5
0

Figure 2

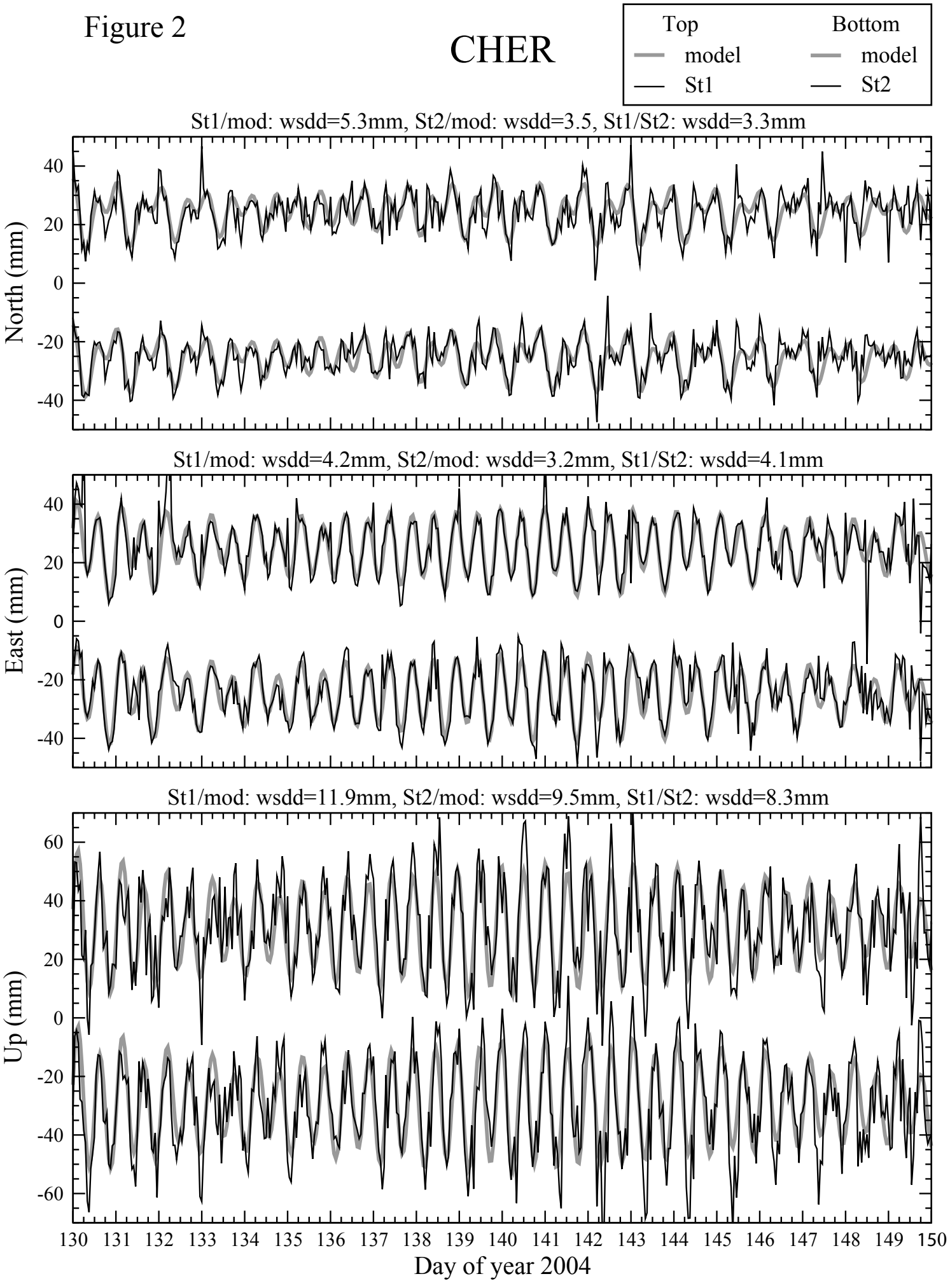
CHER
Top
model
St1
Bottom
model
St2
St1/mod: wsdd=5.3mm, St2/mod: wsdd=3.5, St1/St2: wsdd=3.3mm
North (mm)
St1/mod: wsdd=4.2mm, St2/mod: wsdd=3.2mm, St1/St2: wsdd=4.1mm
East (mm)
St1/mod: wsdd=11.9mm, St2/mod: wsdd=9.5mm, St1/St2: wsdd=8.3mm
Up (mm)
Day of year 2004

Figure 3

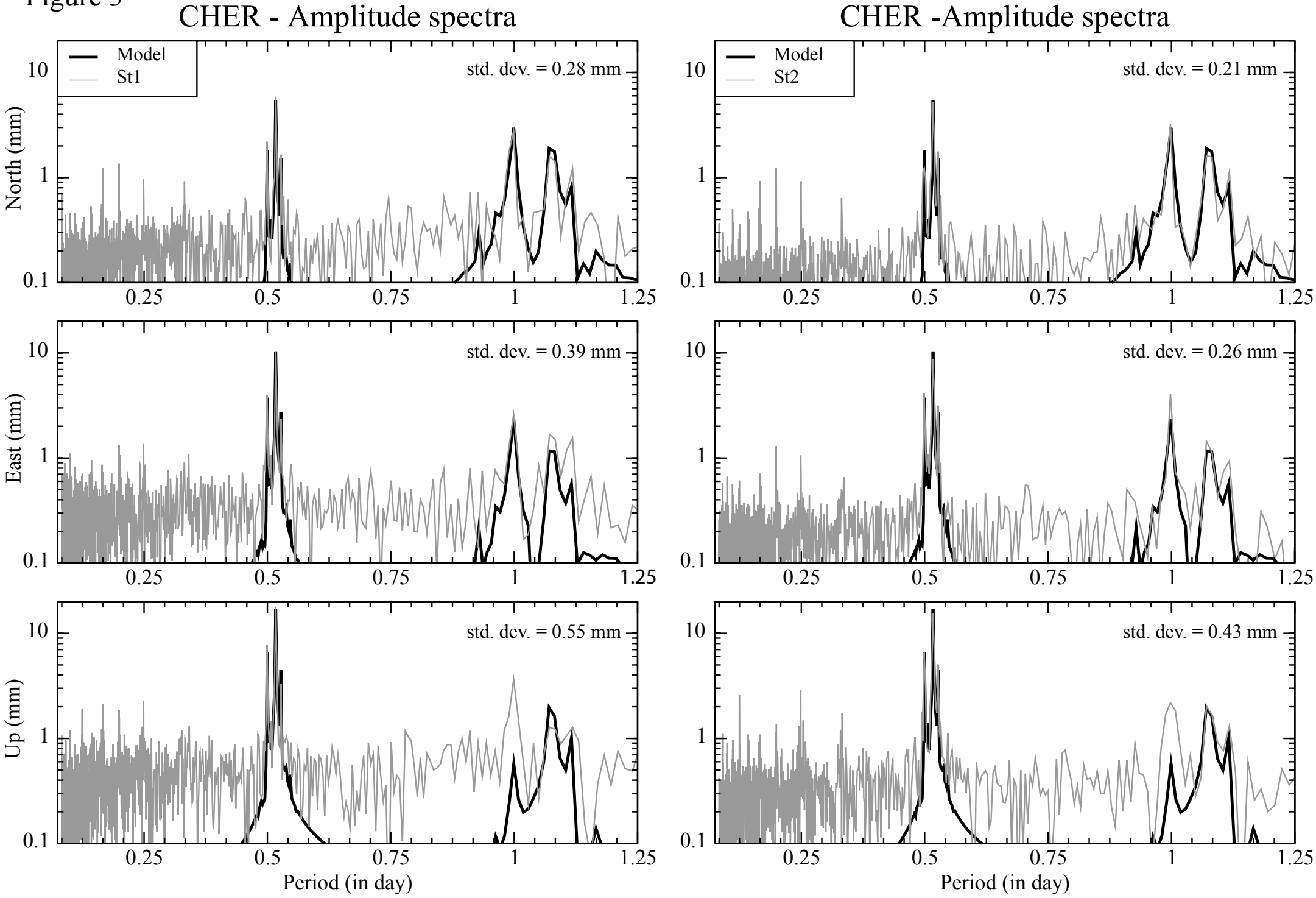
CHER - Amplitude spectra
CHER -Amplitude spectra
Model
St1
St2
std. dev. = 0.28 mm
std. dev. = 0.21 mm
std. dev. = 0.39 mm
std. dev. = 0.26 mm
std. dev. = 0.55 mm
std. dev. = 0.43 mm
North (mm)
East (mm)
Up (mm)
Period (in day)
10
1
0.1
0.25
0.5
0.75
1
1.25

Figure 4

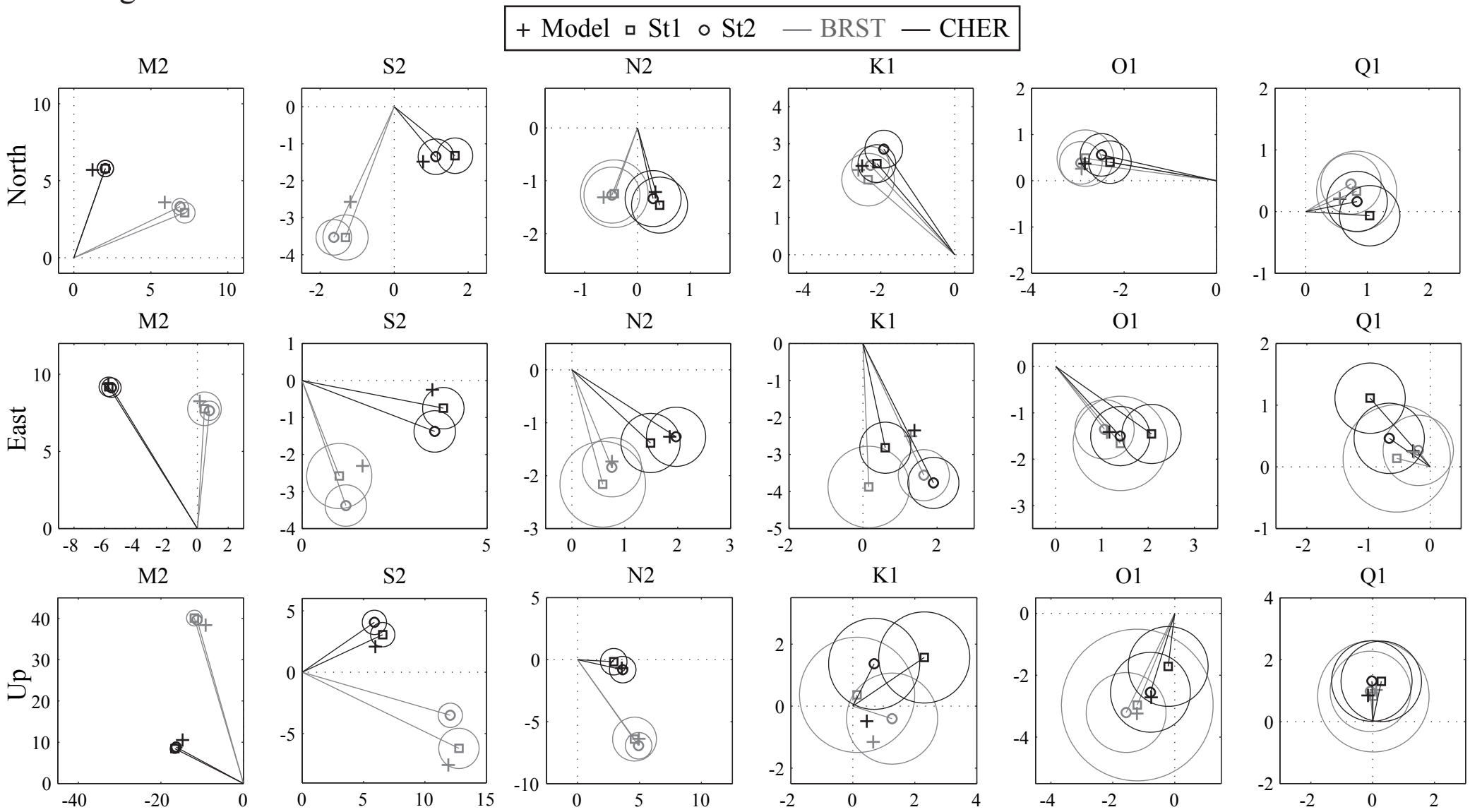

Figure 5

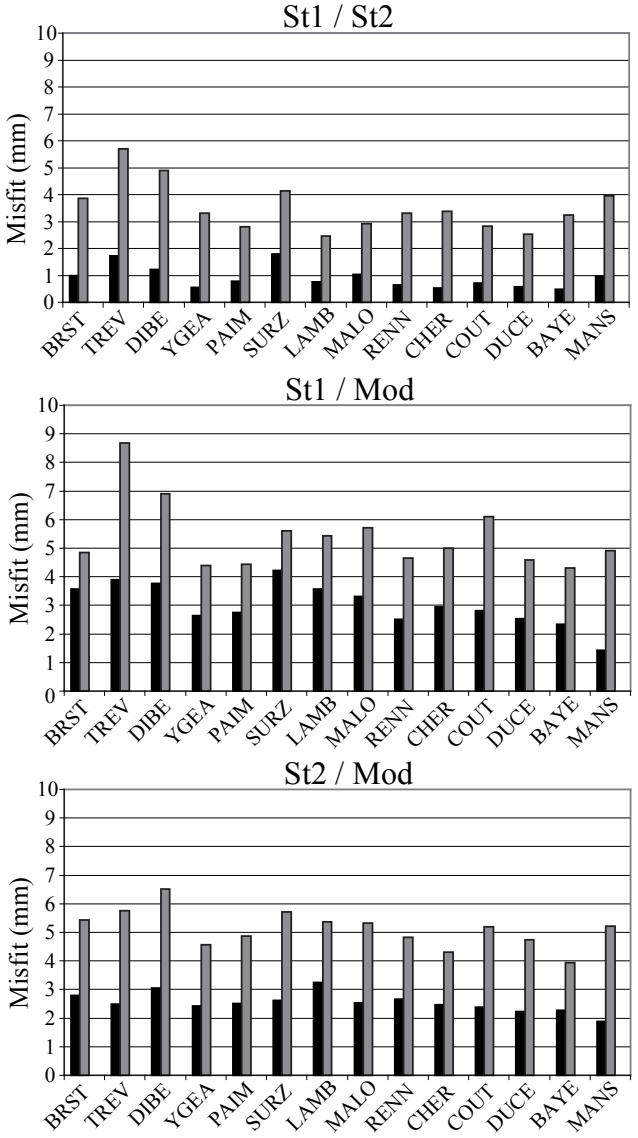
St1 / St2
Misfit (mm)
0
1
2
3
4
5
6
7
8
9
10
BRST
TREV
DIBE
YGEA
PAIM
SURZ
LAMB
MALO
RENN
CHER
COUT
DUCE
BAYE
MANS
St1 / Mod
Misfit (mm)
St2 / Mod
Misfit (mm)

Figure 6

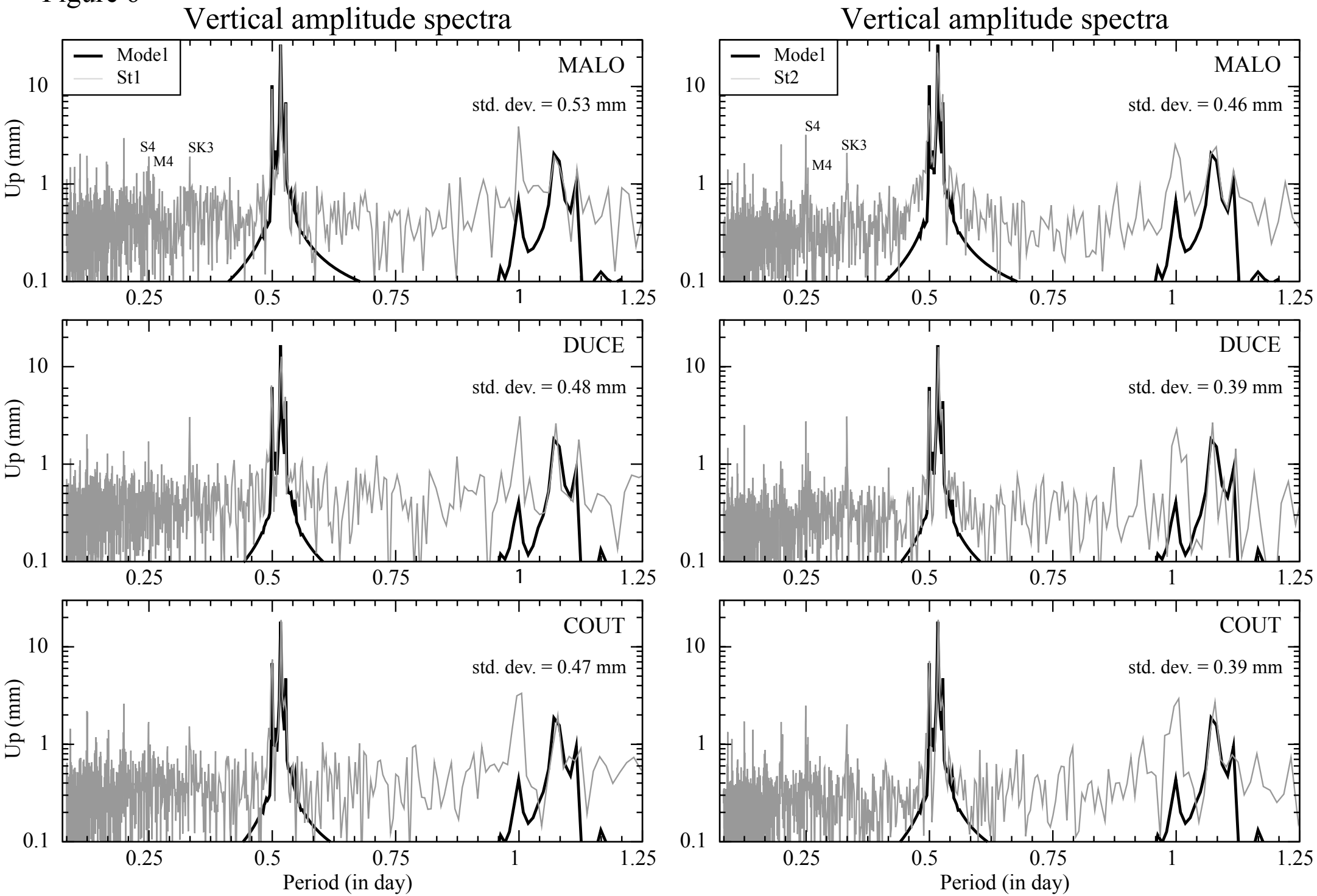
Vertical amplitude spectra
Model
St1
MALO
std. dev. = 0.53 mm
S4
M4
SK3
DUCE
std. dev. = 0.48 mm
COUT
std. dev. = 0.47 mm
Up (mm)
Period (in day)
Vertical amplitude spectra
Model
St2
MALO
std. dev. = 0.46 mm
DUCE
std. dev. = 0.39 mm
COUT
std. dev. = 0.39 mm
Up (mm)
Period (in day)